Turkish Journal of Earth Sciences (Turkish J. Earth Sci.), Vol. 19, 2010, pp. 285–311. Copyright ©TÜBİTAK
doi:10.3906/yer-0902-4 First published online 17 August 2009

Displacements and Kinematics of the February 1, 1944 Gerede Earthquake (North Anatolian Fault System, Turkey): Geodetic and Geological Constraints

MEHMET EMİN AYHAN[1] & ALİ KOÇYİĞİT[2]

[1] Middle East Technical University, Earthquake Studies Department, TR–06531 Ankara, Turkey
(E-mail: meminayhan@gmail.com)
[2] Middle East Technical University, Engineering Faculty, Department of Geological Engineering,
Active Tectonics and Earthquake Research Laboratory, TR–06531 Ankara, Turkey

Received 16 January 2009; revised typescript receipt 11 August 2009; accepted 15 August 2009

Abstract: The North Anatolian Fault System (NAFS) is an approximately 2–110-km-wide, 1600-km-long right-lateral intra-continental transform fault boundary between the Anatolian platelet and the Eurasian plate. The Gerede fault zone is one of the major active structures in the western section of the NAFS. It is a 1–9-km-wide, 325-km-long and ENE-trending dextral strike-slip fault zone, with a total accumulated offset since its initiation (Late Pliocene) of about 43 km. This offset indicates an average geological slip rate of 16.5 mm/yr. The 1 February 1944 Gerede earthquake occurred within the Gerede fault zone. Based on recent field geological mapping of the rupture traces and offsets on it, the average and peak lateral offsets were measured to be 4.37 m and 7.16 m, respectively. A triangulation network covering the region was first set up between 1936 and 1943. Twentyeigth existing points of the network were reoccupied by GPS receivers between 1995 and 2004. Coseismic displacements for the February 1, 1944 Gerede earthquake were obtained at the reoccupation points by removing interseismic deformation and coseismic displacements of recent earthquakes. Modelling the coseismic displacements in elastic half space resulted in a rupture surface slippage of 4.40 ± 0.11 m and 1.02 ± 0.17 m in dextral and normal dip-slip directions, respectively. The 191-km-long and 16-km-deep rupture surface strikes N76°E and dips at 85° ± 5° both to north and south. In the present study the estimated geodetic scalar moment and moment magnitudes are $M_o = 4.02 \times 10^{20}$ Nm and $M_w = 7.74$, respectively. The rupture surface was extended down dip to a depth of about 28 km, and a significant slip distribution was recovered. Based on both the geodetic and geological data, the recurrence intervals for great seismic events to be sourced from the Gerede fault zone were calculated as 232 ± 25 years and 266 ± 35 years, respectively.

Key Words: North Anatolian Fault System, Gerede fault zone, Gerede earthquake, coseismic deformation, GPS, triangulation

1 Şubat 1944 Gerede Depreminin (Kuzey Anadolu Fay Sistemi, Turkiye) Kinematiği ve Yerdeğiştirmeler: Jeodezik ve Jeolojik Kısıtlar

Özet: Kuzey Anadolu Fay Sistemi (KAFS) yaklaşık 2–110 km genişliğinde ve 1600 km uzunluğunda, kıta içi dönüşüm fayı niteliğinde bir levha sınırı olup, Anadolu plakası ve Avrasya plakası arasındaki sınırı oluşturur. Gerede fay zonu KAFS'nin batı kesiminde yeralan önemli aktif yapılardan biri olup 1–9 km genişliğinde, 325 km uzunluğunda, DKD gidişli sağ yanal doğrultu atımlı bir fay zonudur. Oluşumundan (Geç Pliyosen) günümüze değin geçen süre içinde Gerede fay zonunda biriken toplam atım yaklaşık 43 km' dir. Bu toplam atım 16.5 mm/yıl gibi bir ortalama kayma hızına karşılık gelir. 1 Şubat 1944 Gerede depremi Gerede fay zonu içinde oluşmuştur. Ancak bu depremin kinematiği ve kaynak parametreleri tam olarak bilinmemektedir. Jeolojik olarak arazide haritalanan yüzey kırığı ve kırık boyunca atımlara dayalı olarak hesaplanan ortalama sağ yanal atım 4.37 m, yeni ölçülen en büyük sağ yanal atım ise 7.16 m'dir. Çalışma alanı ve çevresini kapsayan triyangulasyon ağı ilkin 1936–1943 yılları arasında kurulmuştur. Bu ağın 28 noktasında 1995–2004 yılları arasında yeni GPS ölçümü yapılmıştır. Intersismik deformasyon ve bölgeyi etkileyen diğer depremlerin kosismik deformasyon etkileri giderildikten sonra, 1944 Gerede depreminin neden olduğu kosismik yer değiştirmeler, yeniden hesaplanmıştır. Kosismik yer değiştirmelerin elastik yarı uzayda modellenmesi, 4.40 ± 0.11 m sağ yanal ve 1.02 ± 0.17 m normal atıma sahip bir yırtılma yüzeyini ortaya koymuştur. 191 km uzunluğunda ve 16 km

derinliğinde olan bu yırtılma yüzeyi K76°D doğrultulu olup yer yer kuzeye ve bazan da güneye 85° ± 5° eğimlidir. 1 Şubat 1944 depreminin jeodezik skaler momenti (M_o)= 4.02x10^{20} Nm, jeodezik moment magnitüdü ise M_w= 7.74 olarak yeniden hesaplanmıştır. Yırtılma yüzeyi aşağı yönde yaklaşık 28 km derinliğe kadar genişletildiğinde önemli kayma dağılımı elde edilmiştir. Ayrıca, Gerede fay zonundan kaynaklanabilecek büyük bir depremin jeodezik ve jeolojik verilere göre yinelenme aralığı da sırayla 232 ± 25 yıl ve 266 ± 35 yıl olarak yeniden hesaplanmıştır.

Anahtar Sözcükler: Kuzey Anadolu Fay Sistemi, Gerede fay zonu, Gerede depremi, kosismik deformasyon, GPS, triyangulasyon

Introduction

The North Anatolian Fault System (NAFS) is an intra-continental transform fault boundary between the Anatolian platelet in the south and the Eurasian plate in the north. It extends from Lake Van in the east to the northern Aegean Sea in the west (Figure 1). A series of devastating recent earthquakes occurred on the NAFS in the 20th century. Due to insufficient operational seismic stations and geological field mapping in the 1940s in Turkey, rupture surface geometry, rupture process and kinematics of the recent seismic events along the NAFS and its geometry could not be clarified satisfactorily (Barka 1996; Ambraseys & Jackson 1998). One of the well-developed structural elements comprising the western half of the NAFS is the Gerede fault zone. The last large seismic event resulting from the reactivation of the Gerede fault zone is the February 1, 1944 Gerede earthquake (Ambraseys & Jackson 1998). Its rupture trace was first examined by Taşman (1944) who reported that the length of rupture and the right-lateral strike-slip and vertical displacements on it are 180 km, 3.5 m and 0.4–1.0 m, respectively. Later on, various aspects of the February 1, 1944 Gerede earthquake were re-examined by several other authors (Ketin 1948, 1969; Ambraseys & Zatopek 1969; Lienkaemper 1984; Öztürk *et al.* 1984; Wells & Coppersmith 1994; Barka 1996; Ambraseys & Jackson 1998; Demirtaş 2000; Herece 2005; Kondo *et al.* 2005). For instance, Kondo *et al.* (2005) reported that the 180-km-long rupture trace occurred along five seismic segments with average right-lateral strike-slip offsets of 1.9–4.3 m. They also reported that the average and peak right-lateral offsets measured along the rupture zone are 3.4 m and 6.3 m, respectively. The magnitude (M_s= 7.3–7.6) and the epicentre location of this earthquake are still being debated (Ergin *et al.* 1967; Ambraseys 1970; Dewey 1976; Jackson & McKenzie 1988; Ambraseys & Jackson 1998). The depth of the February 1, 1944 Gerede earthquake was estimated to be 21.6 km by Jackson & McKenzie (1988). The thicknesses of the seismogenic layer and the crust in this area were reported to be 17 km (Özalaybey *et al.* 2002) and 31 ± 2 km (Zor *et al.* 2006), respectively. It was also suggested that the locking depth is between 15–21 km along the ruptured section of the Gerede fault zone of the NAFS (Nakiboğlu *et al.* 1998; Meade *et al.* 2002; Koçyiğit *et al.* 2006; Reilinger *et al.* 2006). Likewise the total offset accumulated on the Gerede fault zone, its slip rates based on both geological total offset and GPS measurements and the return period of large earthquakes sourced from it were not known well till the present study. In this study we present both new field geological and GPS data to clarify uncertainties about various aspects of the February 1, 1944 Gerede earthquake and the Gerede fault zone. These are mostly the epicentre location, magnitude, ground rupture and its geometry, coseismic offsets along the ground rupture zone, total geologic offset, slip rates on the Gerede fault zone and the return period of large earthquakes to be sourced from it.

We also discuss computed coseismic displacements, modelled rupture surface geometry and slip distribution of the 1944 Gerede earthquake by using geodetic data. A triangulation network, covering the area affected by the earthquake, was first established between 1936 and 1943. Some of its existing points were reoccupied with some GPS receivers from the General Command of Mapping (GCM), Turkey in the period 1995–2004 (Nakiboğlu *et al.* 1998; Kocyigit *et al.* 2006). Coseismic displacements for the 1944 Gerede earthquake were computed at the reoccupation points by removing the effects of both the interseismic displacements

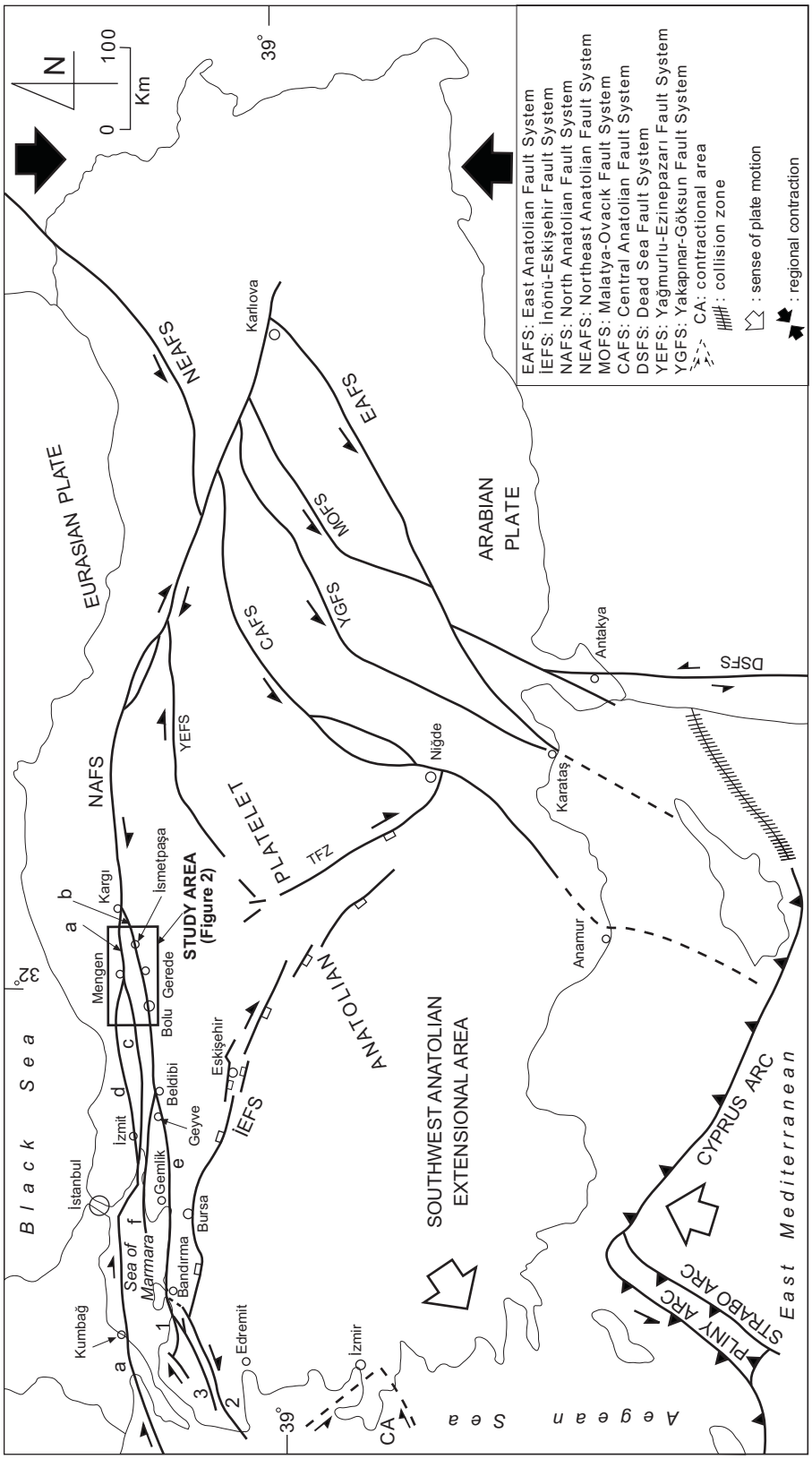

Figure 1. Simplified map showing the major active fault systems in Turkey and adjacent areas. **a**– northern strand of the NAFS, **b**– southern strand of the NAFS, **c**– Mengen-Kaynaşlı-Gölcük fault zone (central strand of the NAFS), **d**– Yığılca-Hendek fault zone, **e**– Geyve-Gemlik fault zone, **f**– Sapanca-Yalova fault zone; **1**– Edincik-Denizkent fault zone, **2**– Yenice-Gönen fault zone, and **3**– Sarıköy-Çan-Bayramiç fault zone.

and the coseismic deformation of the recent events from the geodetic data. Displacements can be inverted in isotropic homogeneous (uniform) or layered elastic half space to obtain rupture surface geometry and slip distribution (Okada 1985; Du *et al.* 1997; Wang *et al.* 2003). Wang *et al.* (2003) have modelled surface displacements of the 1999 İzmit earthquake in both the uniform and layered elastic half space, and found small differences near the rupture traces. GPS displacements of the İzmit event were inverted in both uniform and layered elastic models as well by Hearn & Burgmann (2005) who reported that the layered model provides an increase in scalar moment, centroid depth and maximum slip depth relative to the uniform model. Their distributed slip solutions for the layered elastic models require more slip on and below the high-slip patches. However inversion of surface displacements for deformation due to dislocation in elastically uniform half space is frequently preferred (Arnadottir & Segall 1994; Reilinger *et al.* 2000; Johnson *et al.* 2001; Hreinsdottir *et al.* 2003). For these reasons, in the present study, the rupture surface of the 1944 Gerede earthquake was also modelled as a rectangular dislocation surface in isotropic homogeneous elastic half space. After fixing its geometry and assuming uniform slip, its geodetic strike-and dip-slip components (offsets) and scalar moment were estimated by inversion. To recover slip distribution, first of all, the rupture surface was divided into smaller rectangular surfaces, and their slip components were then obtained by inversion as well. The distributed slip model resulted in geodetic offsets along the rupture trace, and revealed large slip distribution beneath Gerede town. The geodetic recurrence interval was also computed, based on the geodetic offset and geodetic slip rate. The wider distributed slip model revealed significant slips beneath the Gerede rupture surface. The deeper slip implies that post-seismic deformation continued for some period after the February 1, 1944 Gerede earthquake.

Tectonic Setting

As a whole, Turkey is geologically and seismically very complicated. It is currently affected by deformation caused by three contemporaneous neotectonic regimes: strike-slip neotectonic regime, extensional neotectonic regime, and active subduction to contractional neotectonic regime (Figure 1). The strike-slip neotectonic regime prevails through the eastern half and northern part of Turkey, and is dominated by two major structures: the North Anatolian dextral strike-slip fault system (NAFS) and the East Anatolian sinistral strike-slip fault system (EAFS) (Koçyiğit *et al.* 2001). The Anatolian platelet is moving in a WSW direction along these two fault systems, and is overthrusting the easily subducted oceanic lithosphere of the Eastern Mediterranean Sea along the South Aegean subduction zone (Pliny, Strabo and West Cyprus arcs) (Figure 1) since Late Pliocene time (McKenzie 1972; Tokay 1973; Hempton 1987; Koçyiğit *et al.* 2001; ten Veen & Kleinspehn 2002, 2003; ten Veen 2004; ten Veen *et al.* 2004). The third major structure of the strike-slip tectonic regime is the N–S-trending Dead Sea sinistral strike-slip fault system (DSFS). This transform fault separates the African plate in the west from the Arabian plate to the east, and affects the easternmost Mediterranean Sea coastal area including the İskenderun Gulf and Antakya region (Quennell 1958; Freund *et al.* 1970; Bandel 1981; Walley 1988; Mart 1991; McClusky *et al.* 2000) (Figure 1). As well as these major structures, there are also several second order dextral and sinistral strike-slip fault systems, which splay off from the NAFS, cross the Eurasian plate to the Anatolian platelet and deform them internally (Figure 1) (Koçyiğit & Beyhan 1998). The extensional neotectonic regime dominates southwestern Turkey (Koçyiğit *et al.* 1999; Bozkurt 2001). The east and northeast limit of the extensional neotectonic domain is determined by the İnönü-Eskişehir Fault System (İEFS) and the Tuzgölü fault zone (Figure 1). The İnönü-Eskişehir Fault System is predominately a dextral strike-slip fault with a considerable amount of normal component, which forms a transitional zone of deformation between the northern strike-slip and southern extensional domains (Koçyiğit 2005). Starting from this fault system, the type of neotectonic regimes, related structures and stress systems begin to change both to the south and north, with the strike-slip neotectonic regime to the north and the extensional tectonic regime shaped by normal faulting to the south: the İEFS represents

their combination. Likewise, the Tuzgölü fault zone is a dextral strike-slip structure with a considerable normal component. It also forms another transitional belt between the strike-slip and extensional neotectonic domains (Figure 1).

The NAFS cuts through the northern part of Turkey and deforms it intensely. The central part of the NAFS displays a northward convex trace pattern, so that its eastern half trends NW, while its western half trends NE. West of Kargı County, the western half of the NAFS begins to bifurcate into a number of active fault zones, fault sets and isolated faults (a, b, c, d, e, f, 1, 2, 3 in Figure 1). After some distance, they rejoin, re-bifurcate and divide the northwestern margin of the Anatolian platelet into a number of large and small lensoidal crustal blocks, one of which is the Arkotdağ tectonic block (Figure 2). Some of these blocks within the anastomosing strike-slip fault system subside and result in strike-slip basins such as the Sea of Marmara and the north Aegean basins, while others are raised as pressure ridges and push-ups with long axes approximately parallel to the general trend of the NAFS (Şengör *et al.* 1985, 2004; Koçyiğit *et al.* 2006).

The present study area covers the Arkotdağ tectonic block and its immediate surroundings, therefore, in more detail, the Arkotdağ tectonic block is a 10–25-km-wide, 80-km-long and ENE-trending structural highland. It is stratigraphically made up of, from bottom to top, pre-Devonian metamorphic rocks (marble and quartzite) intruded by granite-granodiorite to diorite, Permian dolomitic limestone, an Upper Cretaceous–Lutetian marine sedimentary sequence and Palaeocene–Lower Eocene marine to continental coal-bearing volcano-sedimentary sequence overlain tectonically by a coloured ophiolitic mélange. It is surrounded by several strike-slip basins in the nature of pure strike-slip or superimposed basins with two sedimentary infills of Late Miocene and Early Pliocene age separated by an intervening angular unconformity. These basins are the Bolu, Yeniçağa, Mengen, Eskipazar and İsmetpaşa basins (Figure 2). The Arkotdağ tectonic block is also outlined and determined by the margin-boundary faults of these strike-slip basins, such as the Mengen and Karabük fault zones in the north, the Kadılar fault in the east, the Gerede fault zone in the south and the Çatakören faults in the west (Figure 2).

The Mengen dextral strike-slip fault zone has a considerable amount of reverse component. It is about 7 km wide, 70 km long and trends NE. It is located between Kaynaşlı County in the SW and Mengen County in the NE, and forms the northern margin of the Bolu Basin and the northwestern side of the Arkotdağ tectonic block (Figure 2). The Mengen fault zone consists of a series of parallel and sub-parallel fault segments of dissimilar length. It is an active structure with a geodetically measured slip rate of ~5 mm/yr based on GPS measurements (Koçyiğit *et al.* 2006).

The Karabük reverse fault has a considerable amount of dextral strike-slip component. It is 1–4 km wide, 90 km long and trends NE. It marks the northern side of the Arkotdağ tectonic block (Figure 2). The Karabük fault zone, originally a pre-Miocene southerly verging reverse fault, was reactivated as an oblique-slip reverse fault during the Plio–Quaternary neotectonic period, although, while preserving its earlier nature to some extent it also gained a considerable amount of strike-slip component (Koçyiğit 1987). This fault zone consists of a series of active fault segments, indicated by both the morphotectonic features such as offset stream courses and uplifted to perched terrace deposits and recent seismic activity. The slip rate along this fault zone is ~4 mm/yr based on GPS measurements (Koçyiğit *et al.* 2006).

The Kadılar fault is an oblique-slip normal fault with dextral strike-slip component trending NW and about 30 km long. It consists of two major segments and marks the southwestern margin of the Eskipazar superimposed basin and the eastern side of the Arkotdağ tectonic block. The Kadılar fault is an extensional member of a well-developed dextral strike-slip faulting pattern in this area, and it links the Gerede fault zone with the Karabük and Mengen fault zones (Figure 2).

The Gerede ENE-trending dextral strike-slip fault zone is one of several major fault zones comprising the NAFS. It is 1–9 km wide, and 325 km long extending from Beldibi village in the SW to Kargı County in the NE (b in Figure 1). It bounds the

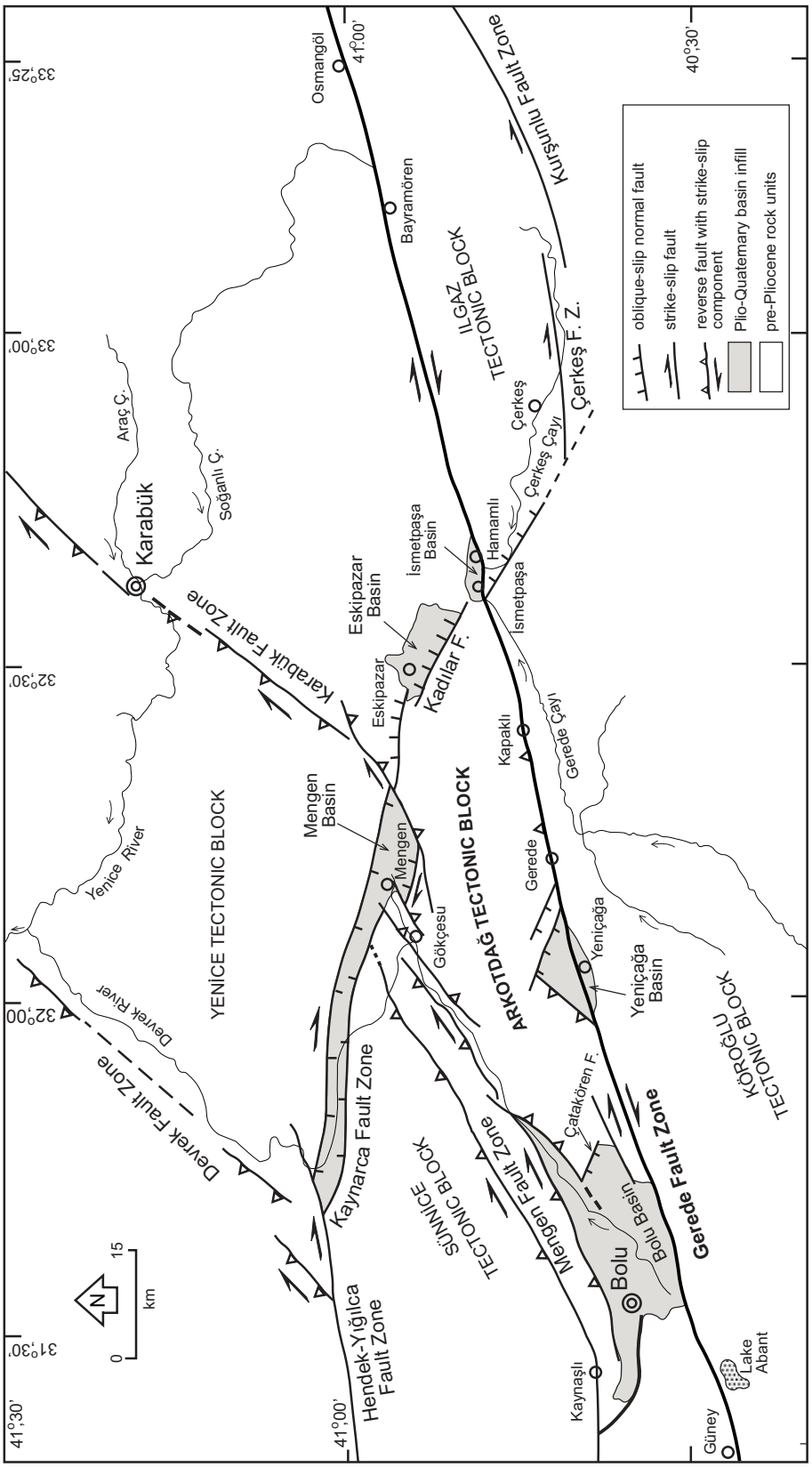

Figure 2. Simplified map showing the Arkodağ tectonic block and adjacent structures.

southern side of the Arkotdağ tectonic block (Figure 2) and consists of a number of parallel and sub-parallel fault segments of various lengths, ranging from 0.4 km to 22 km. It displays an anastomosing type of pattern peculiar to strike-slip faulting, and a series of strike-slip faulting-induced morphotectonic features such as dextrally offset drainage systems, morphotectonic trenches, sag-ponds, pressure ridges, push-ups, perched fault terrace deposits, fault valleys, shutter ridges, fault-parallel aligned alluvial fans and travertine occurrences (Figure 3). The Gerede fault zone also contains the master fault (Y shear) of the NAFS**.** The type locality of the master fault is Gerede County, where it is well exposed and displays a number of strike-slip features; therefore it was named the Gerede fault zone. Total offset accumulated on the Gerede fault zone since its initiation (Late Pliocene: ~2.6 Ma) is about 43 km, based on the offset structural marker, which is the northern boundary of the Eocene volcanic rocks comprising the Galatean arc complex (Koçyiğit *et al.* 2006). An average or uniform slip rate (Keller & Pinter 1996) of ~16.5 mm/yr is obtained when the total offset of 43 km is divided by the elapsed time of 2.6 my. In the same way, the return period of 266 years for large earthquakes to be sourced from the Gerede fault zone is obtained when the averaging coseismic displacement of 4.4 m for the February 1, 1944 Gerede earthquake is divided by the slip rate of 16.5 mm/yr (Koçyiğit *et al.* 2006). Consequently, the total offset of the Gerede fault zone implies to an average slip rate of ~16.5 mm/yr within the Gerede fault zone. This relatively high slip rate of 16.5 mm/yr can produce large earthquakes with magnitude of 7 or higher.

The Çatakören fault is another extensional member of a well-developed dextral strike-slip faulting pattern in this area. It consists of a 5-km-long, closely-spaced and NW-trending high-angle fault segment, located at the eastern tip of the Bolu pull-apart basin. It forms the tectonic contact between the western side of the Arkotdağ tectonic block and the eastern margin of the Bolu Basin (Figure 2).

Based on both GPS measurements (Koçyiğit *et al.* 2006) and the fault-plane solution of the February 1, 1944 Gerede earthquake, the orientation of the principal stress is about NW–SE in and adjacent to the study area. It produced a well-developed dextral

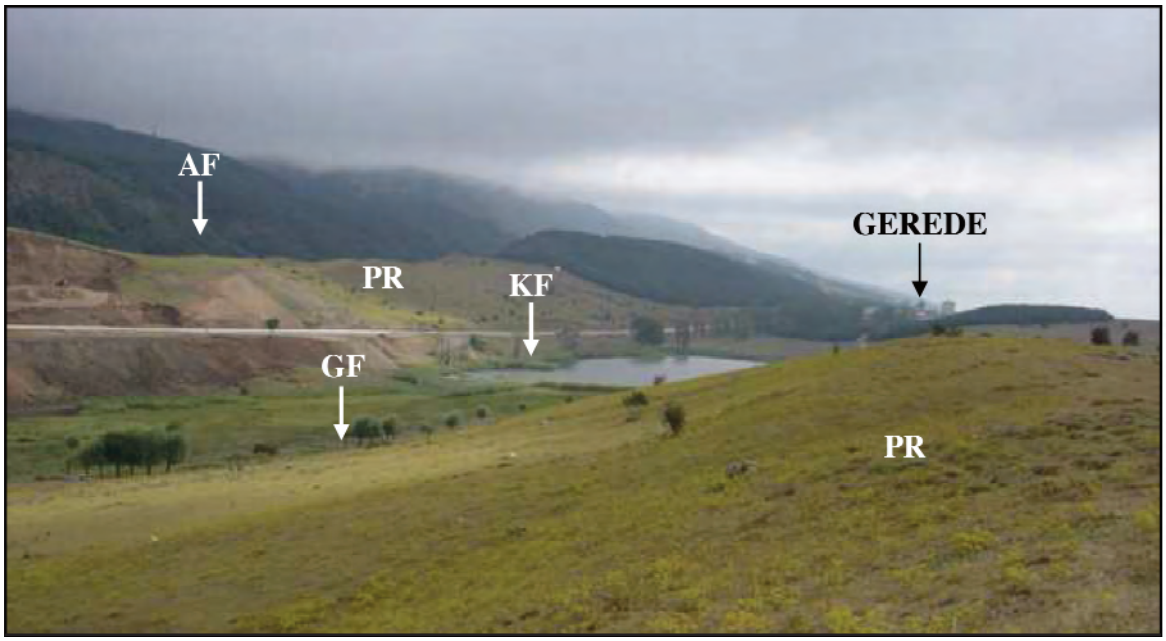

Figure 3. Field photo showing various strike-slip faulting-induced features. PR– pressure ridge, AF– Aksu fault, GF– Gerede fault and KF– Koçumlar fault.

strike-slip faulting pattern in the study area. This pattern consists of NE-trending contractional structures with strike-slip component such as the Mengen and Karabük fault zones, the E–W- and ENE-trending strike-slip structures such as the Gerede fault zone, and the NW-trending oblique-slip normal faults such as the Kadılar and Çatakören faults. In addition, the Gerede fault zone also uses the trace of an older reverse fault in a restricted area between Gerede and Kapaklı, where it has also a reverse component (Figure 2). Consequently, the Arkotdağ tectonic block may be termed as a push up, because it is bounded and controlled by reverse faults and strike-slip faults with a considerable amount of reverse component along its northern and southern margins (Figure 2).

Rupture Trace and Offsets of the February 1, 1944 Gerede Earthquake

Detailed field geological mapping of both the active fault segments and the offset of natural and man-made linear features of the February 1, 1944 Gerede earthquake carried out in the context of the present study indicate that the length of the rupture trace is 195 km (length of natural trace of rupture), and it is located between Güney district in the WSW and Osmangöl in the ENE (Figure 2). We found that the rupture trace consists of 15 structural segments delimited both by bifurcation and double right to left bending of the master fault and rupture zone (Figure 4). The description of individual seismic segments is outside the scope of this paper, because it increases the volume of the paper, and most were previously described to some extent by Kondo *et al.* (2005). During field geological mapping, we identified a number of well-preserved man-made and natural offset linear features. These include concrete or stone walls, fences, field boundaries, lines of trees and stream courses cut and displaced dextrally by the zone of rupture traces (Figure 5).

Nineteen reliable offset features along the whole length of the rupture zone of the Gerede earthquake were examined and measured (numbered 1 through 19 in Figure 4). These measurements indicate: (a) offsets range from 0.7 m to 7.16 m, (b) the peak right-lateral offsets are located approximately along the central part (between Yeniçağa County in the west and Hamamlı village in the east) of the zone of rupture (Figures 4 & 9), (c) the average right-lateral coseismic offset is ~4.4 m. Also noted were: (a) a recurrence interval of 266 ± 35 years for a large earthquake to occur on the Gerede fault zone, based on a slip rate of 16.5 mm/yr, and (b) rupture propagation was generally initiated at a central point, and rupture then continued to both ENE and WSW at a decreasing slip rate along the whole length of zone of rupture (Figures 4 & 9). Evidence of westward and eastward propagation (two-directional propagation) of rupture consists of: (1) the occurrence of peak coseismic displacement at a location close to the epicentre of the earthquake and approximately at the central point of ground rupture (7.16 m at point 6 in Figure 4), (2) in general, a systematic decrease of coseismic displacements to both west and east (Figure 9), and (3) unidirectional propagation is not enough to produce a 195-km-long ground rupture, as indicated by the November 12, 1999 Dağdibi (Düzce) earthquake (Mw= 7.2) with a ground rupture of 40 km.

However, one of the largest coseismic offsets (6.99 m) was measured at point 13, along the rupture zone in the east and outside of the İsmetpaşa aseismic creep site (Figure 4). At first, this appears to be a contradiction between the great offset and the nearby aseismic creep (Aytun 1980). But there is no contradiction, because: (1) the aseismic creep at İsmetpaşa is episodic and very slow (4.5 mm/yr) compared to the slip rate along the Gerede fault zone (geological slip rate is 16.5 mm/yr; geodetic slip rate is 19 mm/yr), so that there is a big difference between the aseismic creep rate and other slip rates; (2) the Gerede fault zone is confined to a very narrow zone (~2 km) in the east and outside the aseismic creep site, and for this reason, much more high elastic strain energy may have been concentrated there, (3) it has not been clarified yet whether the continuing aseismic creep is regional (over 50–70 km) (Çakır *et al.* 2005) or not, (4) the coseismic offset of the 1951 Kurşunlu earthquake may have been superimposed on those of the 1944 Gerede earthquake at point 13, where ground ruptures of both earthquakes overlap, and (5) the appearance of episodic aseismic creep at İsmetpaşa may have been

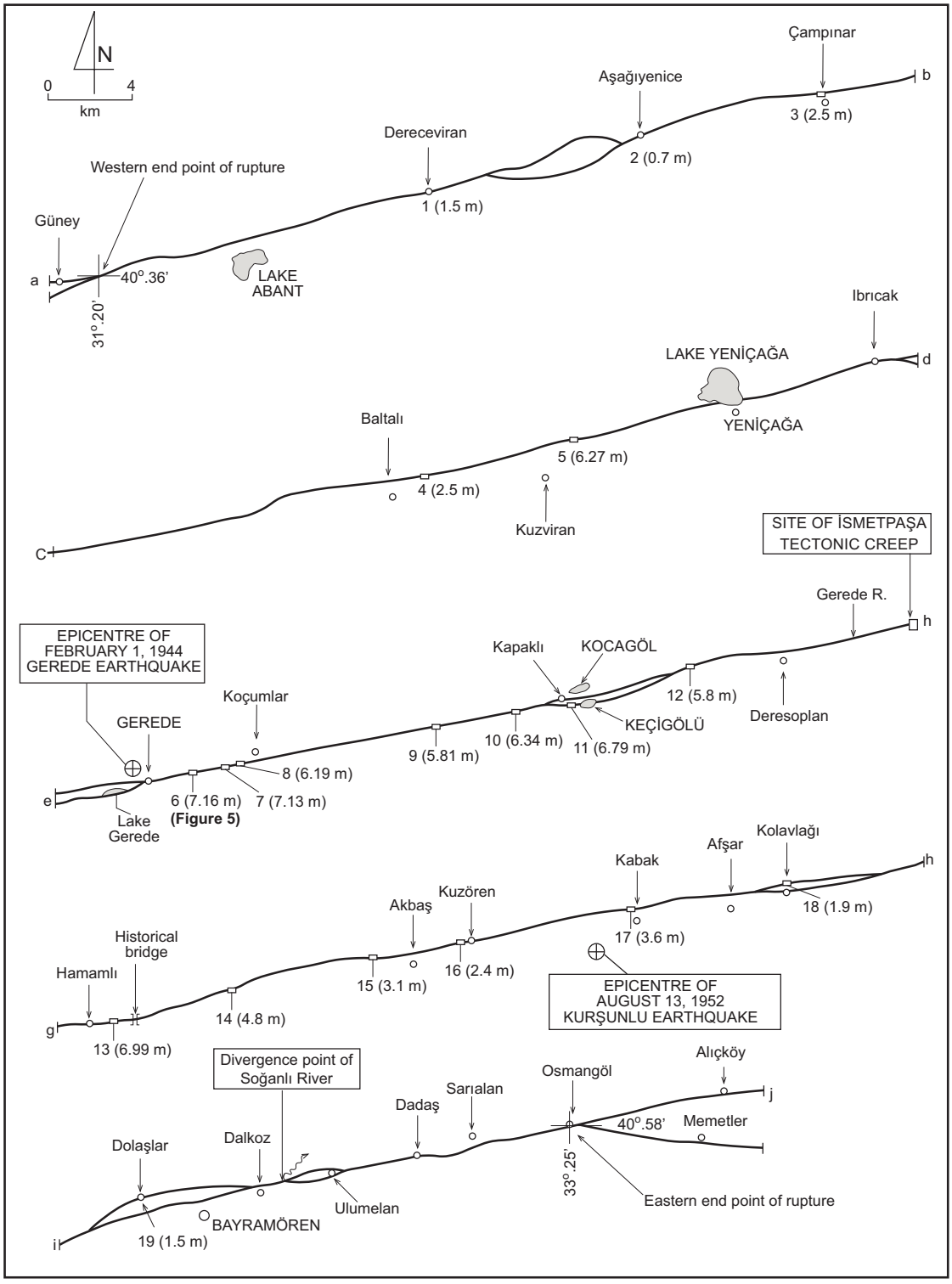

Figure 4. Simplified map showing the rupture trace of the February 1, 1944 Gerede earthquake and various right-lateral offsets measured on it. We presented the geologically measured offsets to one and two decimal places, though their uncertainties may be ± 0.1 m. The likely epicentre location of the Gerede earthquake corresponds to the location suggested by Ergin *et al.* (1967) and Gençoğlu *et al.* (1990).

Figure 5. Field photograph showing a line of trees offset 7.16 m dextrally (A-A') by the February 1, 1944 Gerede earthquake's rupture zone (looking SSE, see Figure 4 for its location).

triggered by the ground rupture-forming large earthquakes such as the 1944 Gerede, 1951 Kurşunlu and the 1999 Gölcük-Arifiye (İzmit) earthquakes.

Geodetic Measurements and Analyses

The basis of our geodetic study is a part of the Turkish fundamental triangulation network, spanning the area limited by latitudes 39.5°–41.75°N and longitudes 29.5°–32.8°E, and first measured between 1936 and 1943. For brevity this network is referred to the 1940 network since most of the measurements were carried out around 1940. The network consists of 126 points and 1015 horizontal directions, three uncalibrated baselines and two astronomical azimuth measurements (Figure 6). The position, orientation and scale of the 1940 network were defined by holding horizontal coordinates (latitude, longitude) of the 7084 and 7213 points. These two points are selected as fixed points since they are deforming similarly within a seismically stable region whose stability is justified by the distribution of earthquakes with magnitude exceeding 4 that occurred between 1973 and 2005 in the study area (Figure 6) (http://neic.usgs.gov/neis). The directions, baselines and azimuths were then adjusted by using the network adjustment software DYNAP (Drews & Snay 1989) and fixing latitude and longitude of the 7084 and 7213 points at their GPS coordinates in the 1995 network (the 1995 network is defined below). On the basis of the points in Table 1, almost evenly distributed across the triangulation network (Figures 6 & 7), average positional uncertainty is about ±0.16 m. The 1940 network is a 2D network referenced to the GRS80 ellipsoid, at epoch 1940, and in the reference frame of the 1995 network. The details of the adjustment to this network are given by Nakiboğlu *et al.* (1998) and Koçyiğit *et al.* (2006).

Two sub-networks consisting of some of the existing points of the 1940 network were occupied by GPS receivers in 1995 (25 points) and from 2002 to

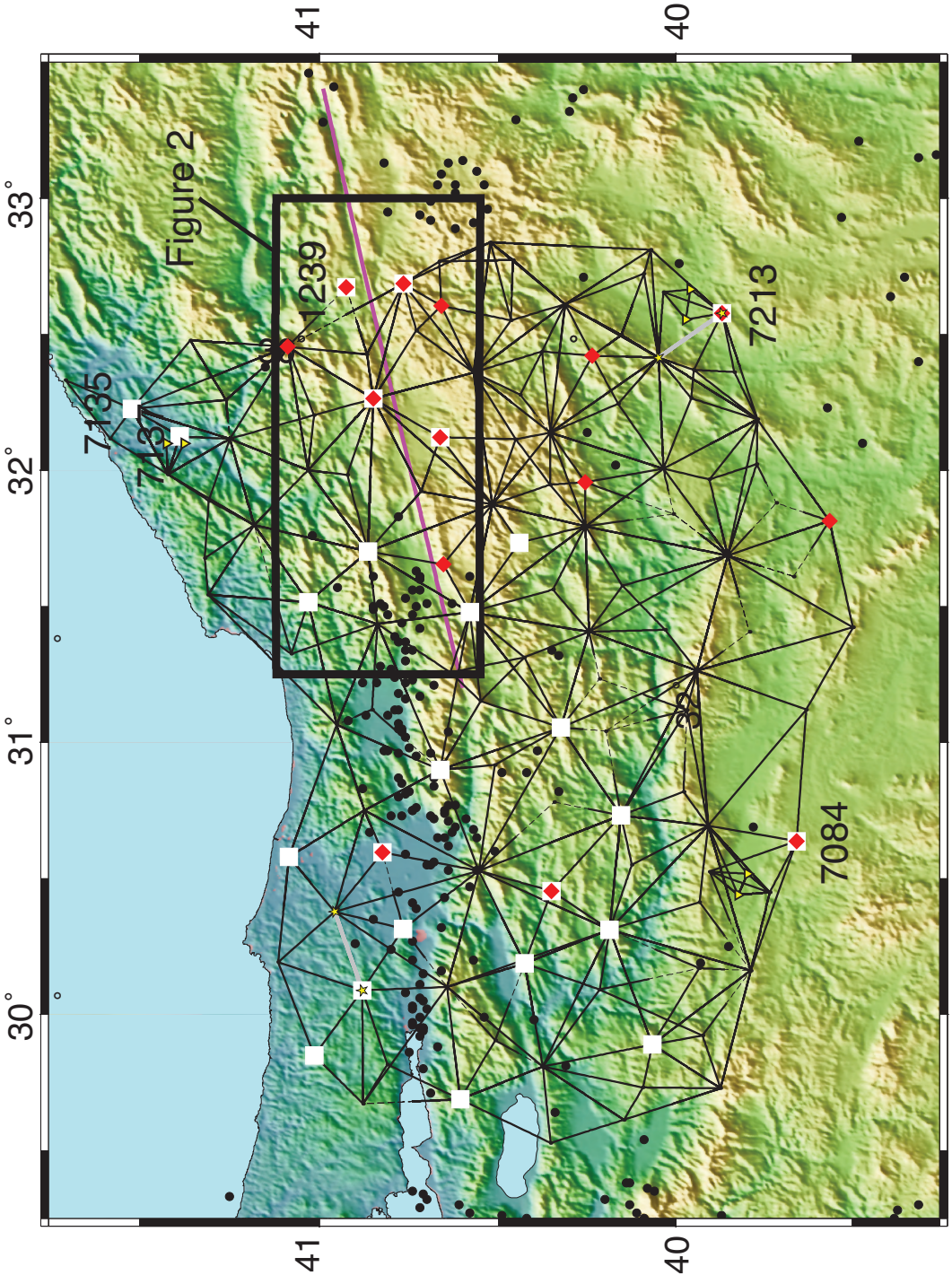

Figure 6. The 1940 network: a part of the Turkish fundamental triangulation network that was established from 1936 to 1943. Solid and solid-dash lines correspond to reciprocal direction and one-sided direction measurements respectively. The grey line is the azimuth measurement line and the yellow star is its end point. The black point is a triangulation point and yellow inverse triangle is the baseline end point. The white square and red diamond are reoccupation points of the 1995 and 2003 networks respectively. The yellow solid circles with black edges are earthquakes with magnitudes exceeding 4 between 1973 and 2005 (http://neic.usgs.gov/neis). The solid pink line and black rectangular box indicate the rupture trace of February 1, 1944 Gerede earthquake and approximately covers the area of Figure 2, respectively.

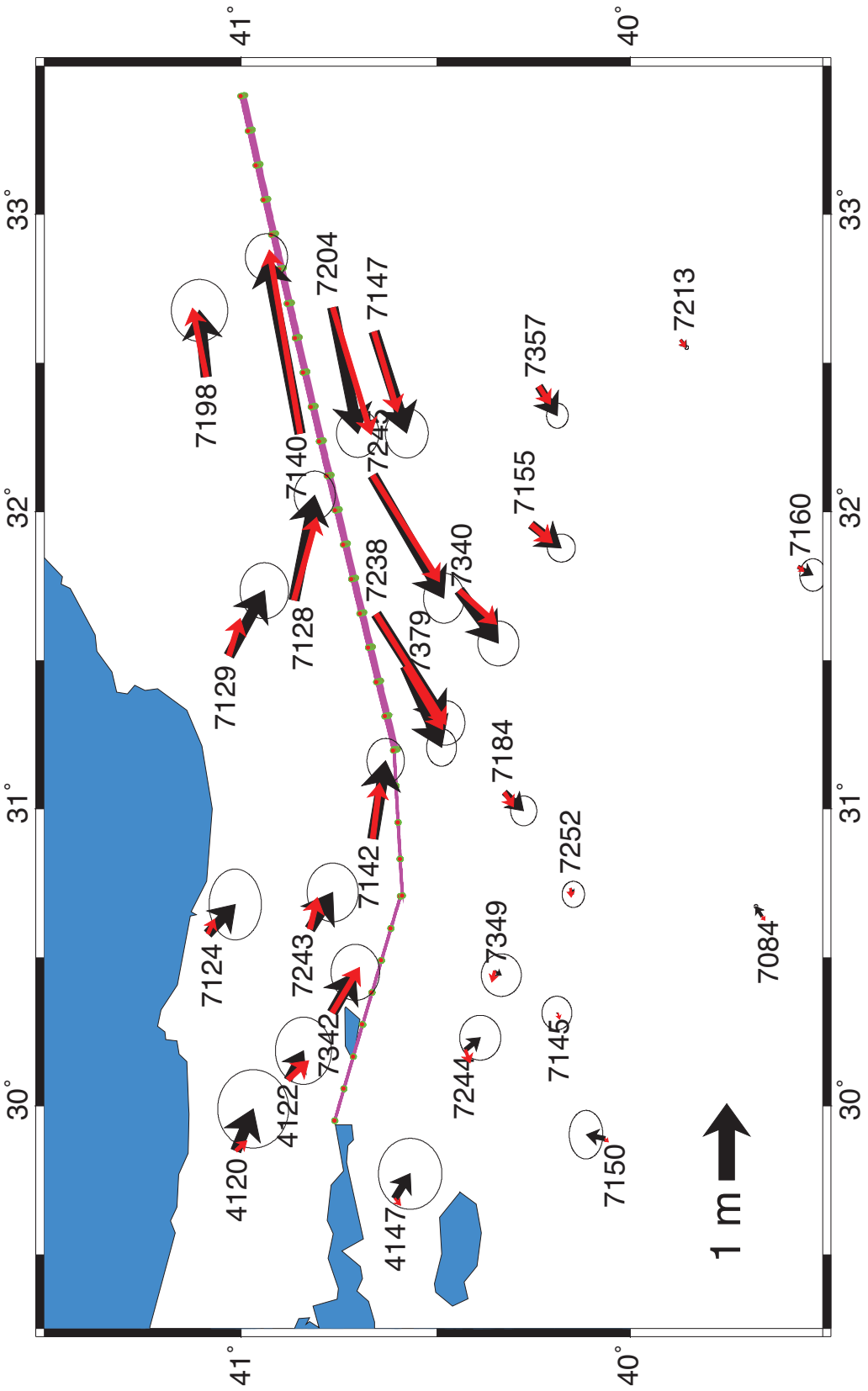

Figure 7. Geodetic coseismic displacements of the February 1, 1944 Gerede earthquake. The black arrow shows the observed displacement. Confidence ellipses show probability of 95%. The yellow arrow is the model displacement. The model displacements were obtained using the distributed slip model which consists of three dislocation surfaces with widths of 16 km. The pink thick lines indicate the surface trace of the dislocation surfaces. The green dots mark the end points of a sub-fault.

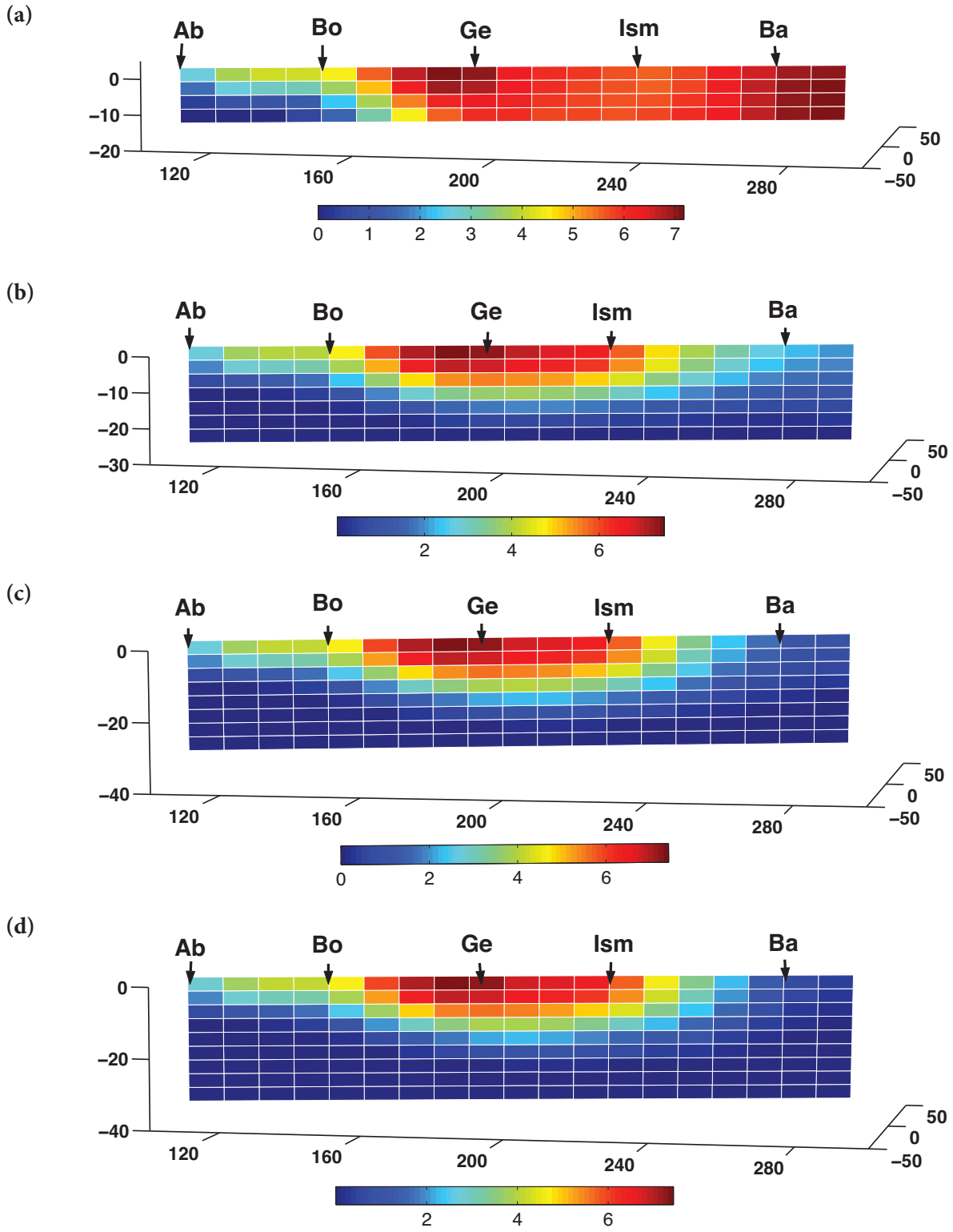

Figure 8. The distributed slip models for the February 1, 1944 Gerede earthquake. Width is **(a)** 16 km; **(b)** 28 km; **(c)** 32 km; **(d)** 36 km. Horizontal and vertical axes are cumulative distance and width respectively in km. Slip is in metres. Ab– Abant, Bo– Bolu, Ge– Gerede, İsm– İsmetpaşa, and Ba– Bayramören.

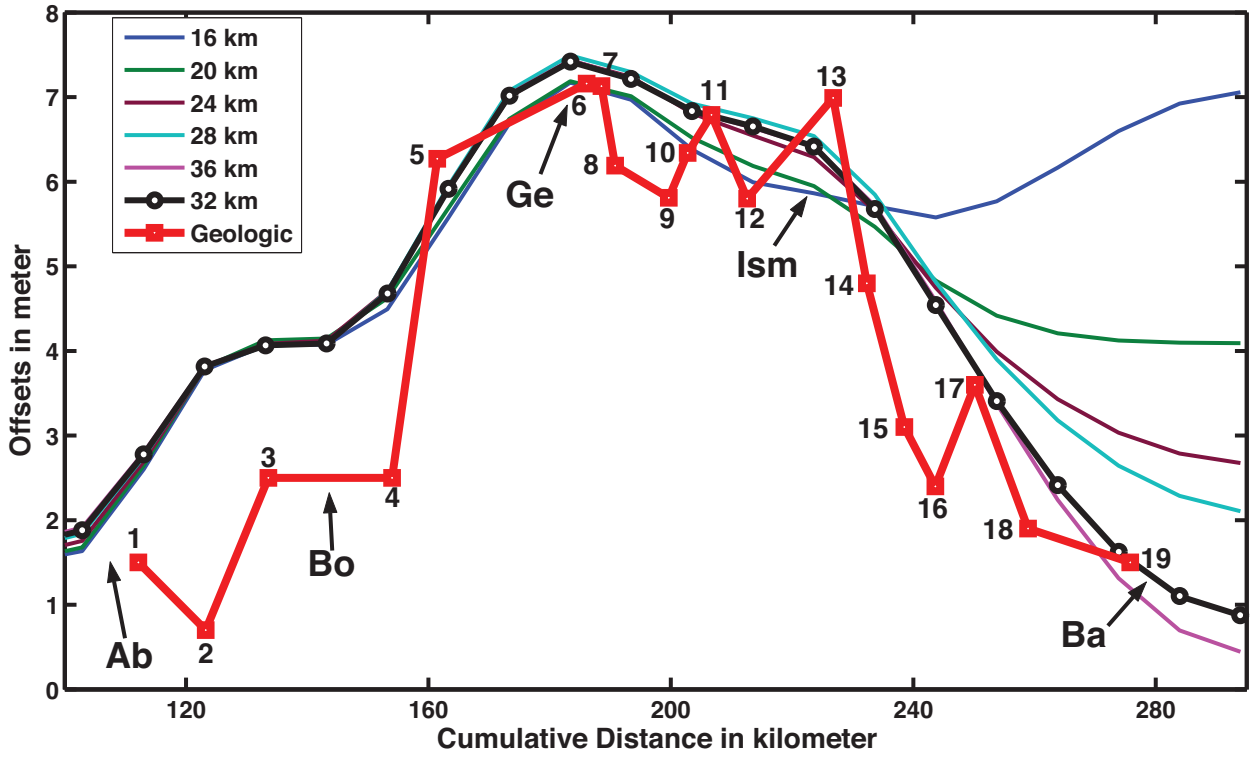

Figure 9. Profiles of the geodetic and geologic offsets along the February 1, 1944 Gerede earthquake rupture trace. Geodetic offsets obtained by distributed slip models with the width of 16, 20, 24, 28, 32 and 36 km are shown in different colours explained in the legend. Circles connected with black lines are of the likeliest distributed slip model with a width of 32 km. Numbered squares in red are the geological offsets illustrated in Figure 4. Ab, Bo, Ge, Ism and Ba are as in Figure 8.

2004 (14 points) (Figure 6) (Nakiboğlu *et al.* 1998; Koçyiğit *et al.* 2006). The GPS campaign measurements were processed by using the Bernese V4.0 software (Rothacher & Mervart 1996). The coordinates of the 25 reoccupation points were computed at 1995 epoch in the ITRF94 reference frame (Nakiboğlu *et al.* 1998). For brevity this network is called the 1995 network. GPS campaign solutions for the years 2002, 2003 and 2004 were combined by using the GLOBK software (Dong *et al.* 1998; Herring 1998), resulting in coordinate estimates of the 14 reoccupation points, at epoch 2003, in the ITRF2000 reference frame (Koçyiğit *et al.* 2006). These 14 points are referred to the 2003 network. Transformation parameters between the ITRF1994 and the ITRF2000 reference frames (ftp://lareg.ensg.ign.fr/pub/itrf/ITRF.TP; McCarthy & Petit 2004) resulted in coordinate differences of about centimetre level at the IGS points included in the both networks. As centimetre level coordinate differences are negligible compared to the average positional uncertainty of the 1940 network, the 1995 and 2003 networks are assumed to be in the same reference frame. The points from both the GPS networks are referenced to the GRS80 ellipsoid, and their horizontal accuracies are less than about ±1 cm.

Coseismic Displacements of the February 1, 1944 Gerede Earthquake

The 1940, 1995, and 2003 networks deal with the February 1, 1944 Gerede earthquake coseismic deformation area at different times but in the same reference frame. Then, horizontal displacements were computed by subtracting horizontal coordinates (latitude and longitude) of the 1940 network from the ones of the 1995 and the 2003 networks at the reoccupation points. The computed

Table 1. Coseismic displacements of the February 1, 1944 Gerede earthquake. σ is standard deviation. In metres.

Point	Latitude	Longitude	East	North	σ_{east}	σ_{north}
4147	40.607	29.688	0.32	−0.20	±0.19	±0.17
4120	41.014	29.849	0.55	−0.23	0.19	0.21
4122	40.880	30.088	0.38	−0.20	0.15	0.18
7084	39.658	30.637	0.13	0.08	0.00	0.00
7124	41.085	30.579	0.38	−0.36	0.14	0.19
7129	41.031	31.515	0.85	−0.46	0.13	0.15
7140	40.850	32.263	2.31	0.44	0.11	0.13
7145	40.187	30.311	0.00	0.02	0.09	0.08
7150	40.066	29.889	0.05	0.25	0.13	0.09
7142	40.663	30.899	1.02	−0.17	0.10	0.12
7184	40.324	31.054	−0.24	−0.25	0.07	0.08
7204	40.766	32.686	−1.65	−0.33	0.11	0.13
7213	39.869	32.577	−0.10	−0.08	0.00	0.00
7243	40.824	30.595	0.48	−0.30	0.14	0.16
7244	40.426	30.187	0.16	−0.19	0.12	0.11
7245	40.663	32.122	−1.61	−0.93	0.11	0.13
7340	40.441	31.734	−0.69	−0.51	0.11	0.12
7252	40.155	30.731	−0.08	−0.04	0.06	0.07
7342	40.766	30.314	0.52	−0.30	0.13	0.15
7349	40.351	30.453	−.05	−0.09	0.11	0.11
7379	40.580	31.479	−1.06	−0.47	0.08	0.10
7128	40.865	31.702	1.38	−0.27	0.11	0.13
7147	40.660	32.605	−1.33	−0.43	0.12	0.13
7155	40.256	31.956	−0.31	−0.39	0.08	0.08
7160	39.564	31.814	−0.11	−0.19	0.09	0.07
7198	41.089	32.454	0.87	0.09	0.15	0.17
7238	40.654	31.654	−1.42	−0.90	0.10	0.12
7357	40.236	32.421	−0.38	−0.24	0.06	0.07

horizontal displacements are called total displacements since they include both interseismic displacements over the intervening interval (1940–1995/2003) and coseismic displacements caused by recent earthquakes that occurred between 1943 and 2003. Due to insufficient data for modelling postseismic displacements, the postseismic deformation was assumed to be represented adequately by interseismic deformation.

Interseismic velocities are required to compute interseismic displacements at the reoccupation points. Repeat GPS measurements have been carried out across all of Turkey since 1988. Interseismic velocities referred to the ITRF2000 reference frame were estimated by processing the GPS campaigns undertaken after 1992 and prior to the 17 August 1999 İzmit earthquake (Aktuğ *et al.* 2004). Then interseismic velocities at the reoccupation points were interpolated from the estimated velocities by using the minimum curvature algorithm since the velocity estimate points mostly do not coincide with the reoccupation points. Finally, assuming linear variation of the interseismic velocities over the intervening interval (55 and 63 years for the 1995

and 2003 networks respectively), interseismic displacements were computed at the reoccupation points by multiplying the interseismic velocity referred to the fixed points with the intervening interval.

Coseismic displacements due to recent earthquakes which occurred during the intervening period require computation of coseismic displacements caused by the recent earthquakes. Bonilla (1988) reported that it is difficult to identify faults which produce earthquakes with magnitude less than 6 by using near surface geological methods, whereas the minimum earthquake magnitude associated with coseismic surface faulting is about 5. We have assumed that earthquakes with magnitude smaller than 6 cause insignificant coseismic displacements at the reoccupation points. The 1940 network spans the interval from 1936 to 1943 while the epoch of the 2003 network is 2003. Therefore the total displacements at the reoccupation points should be corrected for the recent earthquakes (Hendek, Kurşunlu, Abant, Mudurnu, İzmit, and Düzce (Dağdibi)) that occurred between 1943 and 2003 (Table 2). The seismological parameters for the Hendek, Kurşunlu and Abant earthquakes have not been well known since they occurred before the inception of the Worldwide Standardized Seismic Network (WWSSR). The 13 August 1951 (M_s= 6.9) Kurşunlu earthquake was previously reported by several authors, but it has not been mapped (Pınar & Lahn 1952; Ambraseys 1970, 1988; Tokay 1973; Kiratzi 1993; Ambraseys & Jackson 1998). In terms of both the field geological mapping and testimony of villagers who experienced the Kurşunlu event, its rupture zone had followed the approximately 70-km-long Kapaklı-Dalkoz section of the Gerede earthquake rupture zone (Figure 4). For the Mudurnu earthquake, both its rupture trace and offsets were studied by Ambraseys & Zatopek (1969). Furthermore its main shock and aftershock mechanisms were analyzed by Jackson & McKenzie (1988) and Pınar *et al.* (1996). However the rupture trace geometry, offsets and the seismological parameters of the Mudurnu earthquake are still debated. The İzmit and Düzce (Dağdibi) earthquakes were investigated in detail by numerous researchers, and both their epicentre locations and magnitudes were determined. Published epicentre locations and magnitudes for these six recent earthquakes are given in Table 2.

Coseismic displacements due to dislocation across a fault plane in a homogeneous, isotropic and elastic half space are modelled according to Okada (1985). In this model the crust consists of an elastic half space in which plates slide freely along the fault plane. It is assumed that an earthquake ruptured throughout the seismogenic layer in which the fault plane is locked during the interseismic period. Reilinger *et al.* (2006) suggested a locking depth of 15 km within the 1944 Gerede earthquake area by modelling interseismic velocities. The regional locking depth for the 1999 İzmit earthquake area west of the Gerede fault zone was estimated to be 17 km and 21 km by Meade *et al.* (2002) and Reilinger

Table 2. Earthquakes occurred in the study area from 1943 to 2003. M_s and M_w are surface wave magnitude and moment magnitude respectively. [a] : Estimated magnitudes using fault plane geometry parameters (Table 3) according to the dislocation in the elastic theory of Okada (1985). (1) Gençoğlu *et al.* (1990), (2) Jackson & McKenzie (1988), (3) Ambraseys & Jackson (2000), (4) Dewey (1976), (5) USGS-NEIC (http://neic.usgs.gov/neis), (6) Ambraseys (1970), (7) Ambraseys & Jackson (1998).

Earthquakes	Date	Latitude (°)	Longitude (°)	Magnitude	References	M_o (Nm)	M_w
Hendek	June 20, 1943	40.68–40.85	30.48–30.60	M_s= 6.2–6.5	1, 3, 4, 5, 6	9.05×10^{18}	6.64
Kurşunlu	August 13, 1951	40.70–40.90	32.68–33.30	M_s= 6.5–7.1	1, 2, 4, 6, 7	1.35×10^{19}	6.75
Abant	May 26, 1957	40.58–40.67	31.00–31.27	M_s= 7.0–7.2	1, 2, 3, 4, 6, 7	2.84×10^{19}	6.97
Mudurnu	July 22, 1967	40.57–40.70	30.69–31.00	M_s= 6.9–7.3	1, 2, 3, 4, 5, 6, 7	5.73×10^{19}	7.17
İzmit	August 17, 1999	40.70–40.76	29.86–30.00	M_w= 7.4–7.6	1, 3, 5	1.78×10^{20}	7.5
Düzce (Dağdibi)	November 12, 1999	40.74–40.75	31.16–31.21	M_w= 7.2	1, 5	5.53×10^{19}	7.16

et al. (2006) respectively. Koçyiğit *et al.* (2006) found a locking depth of 16 km in the Gerede earthquake area by modelling individually both the coseismic displacements of the February 1, 1944 Gerede event and the interseismic velocities. Furthermore, seismological data discussed in chapter 8 support a seismological layer thickness of about 17 km. We have thus preferred a seismological layer thickness (locking depth) of 16 km within the Gerede fault zone. Forward dislocation modelling requires fault plane geometry parameters: start/end point location, strike, length, width, depth, dip, strike-slip and dip-slip. An earthquake rupture trace usually follows one or more segments whose geometry should be determined from independent seismic, field geological mapping and geodetic data. We defined the segments and their fault plane geometry using geologic field observations only (Table 3). In order to test their reliability, the scalar moment and moment magnitude of each earthquake were computed by using average slip, area of the dislocation surface with a shear modulus (μ) and the formula relating scalar moment to moment magnitude (WGCEP 1995). Feigl & Thatcher (2006) reported that typical values for shear modulus in the Earth's crust range from 30 to 36 GPa, but values as low as 10 GPa and as high as 50 GPa have been used. We have assumed here a shear modulus of 30 GPa, as suggested by Reilinger *et al.* (2000) in modelling the 1999 İzmit earthquake. The computed moment magnitudes presented in the last column of Table 2 are in the range of, or equal to the published earthquake magnitudes in column five. The 1995 network was affected by the Hendek, Kurşunlu, Abant and Mudurnu earthquakes, while the 2003 network was also displaced additionally by the İzmit and Düzce (Dağdibi) earthquakes. Coseismic displacements of each of the recent earthquakes were computed separately with a preferred locking depth of 16 km, and the cumulative coseismic displacements due to the recent earthquakes are obtained at the 1995 and the 2003 network points.

Finally we obtained the February 1, 1944 Gerede earthquake coseismic displacements by subtracting the interseismic displacements and the cumulative coseismic displacements from the total displacements at the 1995 and 2003 network points. Comparison of the coseismic displacements at eight common points of the 1995 and 2003 networks resulted in differences of a few centimetres. Then the Gerede coseismic displacements at the 2003 network points were adapted as coseismic displacement at the common points. Furthermore, the points 7135, 7137 and 1239 in Figure 6 were excluded, since the first two points are inconsistent with both the others and the modelled displacements, and point 1239 was connected weakly to the triangulation network using only two one-sided direction measurements from

Table 3. Segments and parameters of their fault plane geometry for the recent earthquakes occurred in the study area between 1943 and 2003. Data compiled from geological field mapping only are used. [a]: Referred to segment centre.

Segments	Latitude (°)[a]	Longitude (°)[a]	Strike (°)	Length (km)	Width (km)	Depth (km)	Dip (°)	Strike-Slip (m)	Dip-Slip (m)
Hendek	40.8169	30.5176	90	38	16	15.9	95	0.45	-0.20
Kurşunlu	40.8769	32.6880	78	46	16	16.0	88	0.60	0.10
Abant	40.5910	31.0727	80	35.6	16	15.9	96	1.60	-0.40
Mudurnu-1	40.6204	30.5219	102	31.6	16	15.8	80	0.75	0.20
Mudurnu-2	40.5417	30.5203	73	31.5	16	15.9	95	0.50	0.15
Mudurnu-3	40.5898	30.9200	89	36	16	15.9	95	1.90	1.00
İzmit-1	40.7147	29.6963	88	40	16	16.0	88	2.80	1.00
İzmit-2	40.7218	30.1304	89	33.6	16	16.0	92	3.00	-0.75
İzmit-3	40.7103	30.5055	91	40	16	16.0	92	2.80	-1.00
İzmit-4	40.7336	30.8355	69	17	16	14.8	68	1.60	0.25
İzmit-5	40.7836	30.9652	52	8	16	15.5	105	0.12	-0.05
İzmit-6	40.7612	30.9435	87	3	16	15.5	75	0.10	0.02
Düzce-1	40.7676	31.1418	87	36	16	15.5	75	2.75	1.00
Düzce-2	40.7663	31.4556	97	16.4	16	15.9	95	0.40	-0.10

the neighbouring points. The coseismic displacements with their uncertainties at the reoccupation points (28) are given in Table 1 and shown in Figure 7.

Rupture Surface Geometry and Slip Distribution for the February 1, 1944 Gerede Earthquake

The fault rupture surface for the February 1, 1944 Gerede earthquake was modelled as rectangular dislocation surfaces in a homogeneous and isotropic elastic half space (Okada 1985). Assuming uniform slip, geometry of the dislocation surfaces were parameterized by start/end point location, length, depth, width, dip and strike. The parameters were determined in two steps since the displacement points are sparse and unevenly distributed. In the first step the dislocation surfaces were aligned to the geologically mapped rupture traces and their widths were fixed. In the second step the optimum dip angles providing minimum misfit between observed and modelled displacements were computed by forward dislocation modelling. Various dip angles were tested in this step. After fixing the rupture surface geometry the displacements were inverted to estimate strike-slip and dip-slip components of the dislocation surfaces. The model includes three dislocation surfaces: one in the east follows the rupture trace of the 1944 Gerede earthquake, and the other two in the west are almost coincident with the rupture trace of the Mudurnu and Abant earthquakes. The parameters of these three dislocation surfaces are given in Table 4. In order to quantify the contribution of each dislocation surface, displacements were computed at the sub-network points for each dislocation surface by individual forward dislocation modelling. We found that the eastern dislocation surface accounts for 96% of the displacements, whereas the rest were caused by the other two dislocation surfaces in the west. The eastern dislocation surface, corresponding to the February 1, 1944 Gerede earthquake, dips 85 ± 5° to the north and south in places, slipped 4.40 ± 0.11 m dextrally and 1.02 ± 0.17 m dip slip northern and southern sides down respectively, north side down, extends down-dip width to 16 km, and has a length of 191 km (length of straightened trace of rupture) (Table 4). The geodetic scalar moment and corresponding moment magnitude were found to be M_o= 4.13x10^{20} Nm (Newton-meter) and M_w= 7.74 respectively with shear modulus (μ) of 30 GPa.

Furthermore, to resolve more detailed distributed slip, the three dislocation surfaces were divided into 10-km-long and 4-km-wide sub-faults. Each sub-

Table 4. Modelled dislocation surface geometry parameters and distributed slip estimates for the February 1, 1944 Gerede earthquake. The Gerede and Gerede Distributed Slip models correspond to the eastern dislocation surface. Latitude and longitude are referred to the centre of the dislocation rupture trace: wrss is weighted residual sum of squares. Patch– number of sub-faults along and dip of dislocation surface, Para.– number of unknowns and Meas.– number of measurements.

Model	Latitude (°)	Longitude (°)	Strike (°)	Length (km)	Width (km)	Dip (°)	Strike-Slip(m)	Dip-Slip(m)	wrss	M_w	M_o (10^{20} Nm)
3 faults	40.675	30.327	106	67	16	89	1.62 ± 0.25	0.00 ± 0.00	809	7.79	4.82
Uniform	40.597	30.954	87	42	16	89	1.37 ± 0.25	0.17 ± 0.33			
Slip Model	40.795	32.301	76	191	16	85	4.40 ± 0.11	1.02 ± 0.17			
Gerede	40.795	32.301	76	191	16	85	4.40 ± 0.11	1.02 ± 0.17	–	7.74	4.02
	Patch	**Size (km)**	**Para.**	**Meas.**							
3 faults	4 × 30	4 × 10	240	56	16				599	7.82	5.38
Distributed	7 × 30	4 × 10	420	56	28				579	7.78	4.65
Slip Model	8 × 30	4 × 10	480	56	32				575	7.77	4.56
	9 × 30	4 × 10	540	56	36				572	7.77	4.58
Gerede	4 × 19	4 × 10	76	56	16				–	7.77	4.57
Distributed	7 × 19	4 × 10	133	56	28				–	7.7	3.54
Slip Model	8 × 19	4 × 10	152	56	32				–	7.68	3.36
	9 × 19	4 × 10	171	56	36				–	7.68	3.29

fault has two unknowns: one right-lateral strike-slip and one normal dip-slip. However, in this case the inversion is ill posed since the number of observations is smaller than the number of unknown slips. To regularize the ill-posed inversion and avoiding the estimated slip distribution to become oscillatory, smoothing and non-negativity constraints were introduced (Lawson & Hanson 1974; Harris & Segall 1987; Du *et al.* 1992, 1997; Arnadottir & Segall 1994). The coseismic displacements were then inverted for the optimal slip distribution model maintaining a small misfit between the modelled and observed coseismic displacements. The computed slip distribution model displacements at the reoccupation points are shown in Figure 7. The modelled displacements are satisfactorily coincident with the observed displacements. Figure 8a shows the dextral strike-slip distribution across the dislocation surface for the width of 16 km. Two maximum slip areas were recovered in Figure 8a: one around Gerede and one at the east end of the rupture plane. The slip decays smoothly towards the west and down-dip between Bolu and Lake Abant, whereas significant slips are obtained towards the east end and particularly along the bottom edge. This pattern is not compatible with that of the geological offsets which gradually taper to zero at both the east and west ends and have high values in the central section of the rupture (Figure 4). Incompatibility of the geodetic and geologic offsets and slip not diminishing at both the east end and the bottom edge imply modification of the dislocation surface. Extending the dislocation surface to the east may not be remarkable since the east end of the rupture trace was precisely mapped in the field. We then concluded that the distributed slip model implies an additional slip beneath the dislocation surface. Zor *et al.* (2006) reported average crustal thickness of 31 ± 2 km for the eastern Marmara region using teleseismic receiver functions. The down-dip width of rupture surfaces was increased in increments of 4 km from 16 km to 36 km. Figure 8a–d illustrate dextral strike-slip distribution for widths of 16, 28, 32 and 36 km, and their related parameters (wrss, M_w, M_o) are given in Table 4. Significant changes of the slip distribution pattern are evident for the models with widths equal to or exceeding 28 km. These models have only one shallow maximum slip area around Gerede, with smoothly diminishing slip towards both the east and west ends, and tapering to zero along the bottom edge of the dislocation surface. In order to investigate how much additional information was recovered by the distributed slip models relative to the uniform slip model, we first made comparisons on the basis of the wrss. The distributed slip models reduced the wrss by 28%. Furthermore RMS of the discrepancy between modelled and observed displacements were found to be ±0.24 m and about ±0.17 m for the uniform slip model, and the distributed slip models respectively. Consequently, it is evident that the distributed slip models recover more details than the uniform slip model.

Discussion

In order to define the most appropriate distributed slip model, the estimated fault slips (geodetic offsets) were first compared to each other and then to the geological offsets along the Gerede rupture trace. The geodetic offset profiles for widths of 16, 20, 24, 28, 32 and 36 km and the geologic offset profile are shown in Figure 9. The geodetic profiles are smooth and almost coincident with each other between Lake Abant and east of İsmetpaşa but they differ significantly towards the east end. East of İsmetpaşa, the 16, 20, 24, 28, 32 and 36 km profiles decay smoothly to about 7.1, 4.1, 2.7, 2.1, 0.9 and 0.4 m respectively at the east end. In the west, unlike in the east, all the profiles attenuate smoothly to 1.60–1.85 m. Dispersion of the profiles in the east of İsmetpaşa may be caused basically by sensitivity of the inversion algorithm to the lack of observation points there. The geological offsets have local scatter in general and taper to small values at both ends following a parabolic concave course. They tend to be less than the geodetic estimates along the rupture trace except within the central section, between locations 5 and 13, where the geologic and geodetic offsets are almost identical. Only the profiles with widths of 32 and 36 km satisfy this pattern. Thatcher *et al.* (1997) pointed out that the ratio of geological to geodetic offsets averages 80%. We obtained here a ratio of about 84% for the whole rupture trace (excluding locations 5 and 13). Thatcher & Lisowski (1987) reported that geodetic offsets are usually greater than geological offsets since geological offset

is usually measured along the master fault, even if the deformation is distributed within the deformation zone. Such is the case for the Gerede earthquake, since the Gerede fault zone consists of a 1–9-km-wide belt of deformation containing numerous active fault traces of considerable complexity and along-strike variability. Large geological and geodetic offsets are localized around Gerede. The geodetic peak offsets, varying between 7.17 and 7.49 m, are larger than the geological peak offset (7.16 m). The geodetic peak offsets of 7.49 m and 7.41 m were obtained for the model of 28 km and 32 km, respectively. Furthermore, we investigated slip distribution within the strip of sub-faults at depths between ~24 km and ~28 km (Figures 8b–d). This strip is common for the models of depths of 28, 32 and 36 km. Both the models for 32 km and 36 km recover approximate decimetre level slip beneath the section from west of Gerede to Bayramören and no slip deeper than 28 km, whereas the 28 km model estimates a few centimetres of slip beneath both Gerede and at the east end. We also found that the contribution of the 36 km model is insignificant relative to the 32 km model. Consequently, the slip patterns for the models at depths of 28, 32 and 36 km in Figure 8, comparisons of the geodetic to geologic offset profiles and slip distribution within the strip at depths between ~24 km and ~28 km reveal that the distributed slip model at the 32 km depth may be more satisfactory. Hence we preferred here the model with the width of 32 km as the most appropriate distributed slip model for the Gerede earthquake. However we should note that the 32 km model recovers slip confined to the layer between the surface and a depth of ~28 km (Figure 8c).

Geological offset is significantly larger than geodetic offset at location 13, within the İsmetpaşa basin. Ambraseys (1970) and Aytun (1980) reported aseismic creep on the NAFS at İsmetpaşa moving at a rate of about 1 cm/yr. Çakır *et al.* (2005) suggested aseismic creep along a 70 km section of the NAFS centred on İsmetpaşa. The aseismic creep at and around İsmetpaşa may cause additional geological offset at this location. Furthermore the measured geological offset at location 13 may include the offset caused by the Kurşunlu earthquake since the rupture trace of the Kurşunlu event runs parallel to the Gerede rupture and coincides with it at some locations between Kapaklı and Dalkoz (Figure 4).

The seismogenic layer thickness (locking depth) of 16 km was suggested previously on the basis of available studies using GPS data. Furthermore, the foci of aftershocks of the 17 August 1999 İzmit and 12 November 1999 Düzce earthquakes were confined to the upper ~17 km of the upper crust (Örgülü & Aktar 2001; Tibi *et al.* 2001; Özalaybey *et al.* 2002). Earthquakes with magnitude exceeding 4, which occurred in this area since the 1970s (http://www.globalcmt.org and http://neic.usgs.gov/neis) support the suggested thickness as well. Hence previous GPS studies and seismic data available do reveal that the locking depth of about 16 km is remarkable in the Gerede earthquake area. If so, what causes the slip recovered by the most appropriate distributed slip model within the ~12-km-thick layer underlying the 16-km-thick seismogenic layer? Kenner & Segall (2000) suggested that great strike-slip earthquakes may cause postseismic afterslip on the rupture surface and its down dip extension, and trigger postseismic relaxation of the lower crust and asthenosphere. Thatcher (1975) found slip of 3–4 m below the 10-km-thick seismogenic layer to depths of ~30 km for the 1906 San Francisco earthquake by using post earthquake triangulation data from 1906 to 1930. Hearn *et al.* (2002) modelled slip down to 25 km for recent earthquakes along the NAFS to provide allowance for afterslip deeper in the crust than the coseismic rupture. Furthermore distributed postseismic strike-slip during the first 75 days after the 17 August 1999 İzmit earthquake was modelled by Reilinger *et al.* (2000) with a model of fault geometry identical to the coseismic model, but extended to a depth of 40 km. Hence we suggest that the slip confined to depths between ~16 km and ~28 km beneath the rupture surface provides evidence of continuing deformation for some period after the Gerede earthquake. Hence we think that a layer of lower crust at depths between ~16 km and ~28 km accommodates pronounced postseismic afterslip and relaxation effects, while coseismic slips are confined to the ~16 km thick seismogenic layer.

The epicentre location of the 1944 Gerede earthquake was previously reported to be outside and about 30 km north of the rupture trace zone (Ambraseys & Zapotek 1969; Ambraseys 1970; Aslan *et al.* 1975; Dewey 1976; Kalafat 1998). Ergin *et al.* (1967) located the epicentre WNW of, and very close

to Gerede, while Ambraseys & Jackson (1998) suggested it was NW of, and near İsmetpaşa. The dominating features of the most appropriate distributed slip model are centred around Gerede and with slip diminishing progressively towards the east and west and the bottom edge (Figure 8c). Furthermore, the geological and geodetic peak offsets are concentrated around Gerede (Figures 4 & 9). Therefore we suggest that the epicentre location of the February 1, 1944 Gerede earthquake was just east of Gerede. The epicentre locations proposed by various authors and the one suggested here are all shown in Figure 10.

Jackson & McKenzie (1988) suggested a fault plane solution for the 1944 Gerede earthquake consisting of a pure strike-slip vertical dislocation

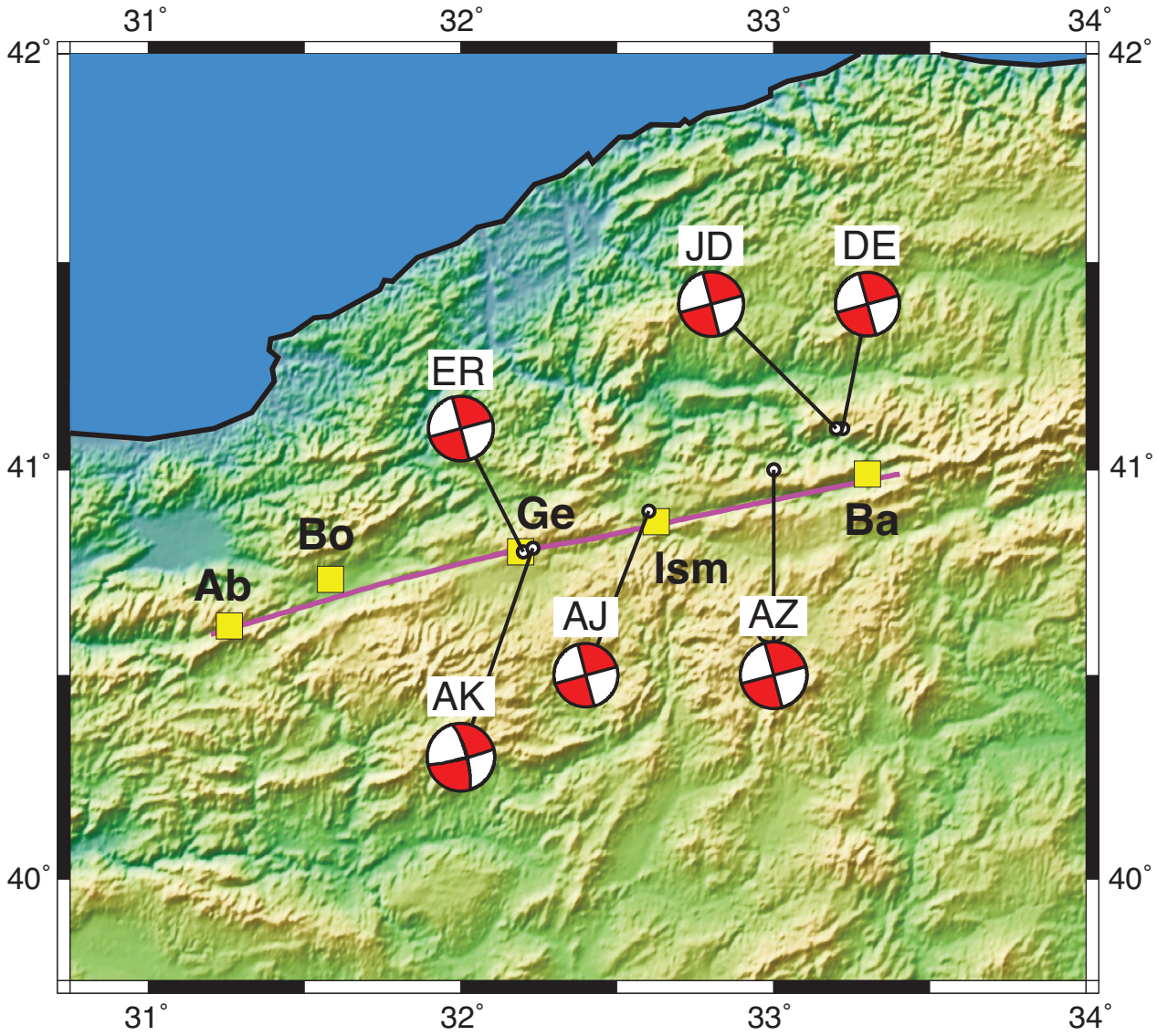

Figure 10. Proposed epicentre locations for the 1944 Gerede earthquake (white circle): AJ– Ambraseys & Jackson (1998), AK– this paper, AZ– Ambraseys & Zatopek (1969), DE– Dewey (1976), ER– Ergin *et al.* (1967), JD– Jackson & McKenzie (1988). The beachball estimated by Jackson & McKenzie (1988) was used for each epicentre except AK which was prepared by using the parameters for the Gerede rupture surface in Table 4. Yellow squares indicates cities or towns. The pink thick line is the rupture trace of the February 1, 1944 Gerede earthquake. Ab, Bo, Ge, Ism and Ba are as in Figure 8.

plane with a depth of 21.6 km and seismic scalar moment (M_o) of 2.16–4.31x10^{20} Nm, respectively. Corresponding seismic moment magnitude of 7.56–7.76 was computed by using the relationship M_w= (2/3) $\log_{10}$ (M_o) – 6 (WGCEP 1995). Furthermore, depending on the rupture length of 191 km, we found M_w= 7.71, M_o= 3.73 × 10^{20} Nm, width= 21.04 km, maximum surface offset= 8.25 m, and average offset= 4.20 m for the February 1, 1944 Gerede earthquake by using the empirical regression equations for strike-slip earthquakes (Wells & Coppersmith 1994; WGCEP 1995). The estimated geodetic scalar moment and moment magnitude for the uniform slip model are 4.02 × 10^{20} Nm and 7.737, respectively. We also computed scalar moment and moment magnitude for the distributed slip models (Table 4). The geodetic scalar moments agree with the seismic and empirical moments. The lowest M_s= 7.3 (M_w= 7.39) proposed by both Dewey (1976) and Ambraseys & Jackson (1998) is significantly lower than the seismic, empirical and geodetic moments which vary in the range of M_s= 7.4–7.65 (M_w= 7.49–7.76).

Ketin (1948), Ambraseys & Zatopek (1969) and Ambraseys & Jackson (1998) reported peak offsets of 3.5–3.7 m which are about half the geodetic, empirical and recently measured geologic peak offsets which range from 6.3 to 8.25 m. The empirical average offset agrees with both the average geological and geodetic offsets obtained in this study, whereas they are about one metre larger than the value suggested by Kondo *et al.* (2005).

The February 1, 1944 Gerede earthquake moment, epicentre locations and fault plane parameters suggested by various authors and in this paper are presented in Table 5.

The slip rate along the NAFS was estimated as 24 ± 1 mm/yr from best fitting Euler vector by McClusky *et al.* (2000) using recent GPS observations carried out between1988 and 1997. Hearn *et al.* (2002) discussed the slip rates for the NAFS computed by different research groups and suggested that the slip rate must be about 24 mm/yr. However Ayhan *et al.* (2002) and Koçyiğit *et al.* (2006) computed slip rate of 17 mm/yr and ~19 ± 2 mm/yr, respectively for the Bolu-İsmetpaşa section of the Gerede fault zone by using interseismic GPS velocities. The geodetic recurrence interval for great seismic events to be sourced from the Gerede fault zone is 232 ± 25 yr when we use a GPS slip rate of 19 mm/yr and a geodetic lateral strike-slip of 4.40 ± 0.11 m for the uniform slip model.

Conclusions

In general, geodetic data around the rupture trace provide valuable information on the coseismic deformation and the rupture surface geometry of an earthquake which occurred before the inception of modern instrumental period. The February 1, 1944 Gerede earthquake was investigated by using triangulation, GPS and geologic offset measurements. We conclude that the rupture surface, located between Lake Abant in the west and Osmangöl (Bayramören) in the east, dips northward and southward at 85° ± 5°, is 191 km long and 16 km wide. Its right-lateral strike-slip and normal dip-slip components, geodetic scalar moment and moment magnitude are 4.40 ± 0.11m, 1.02 ± 0.17 m, M_o= 4.02 × 10^{20} Nm, and M_w= 7.74, respectively.

In the distributed slip model, the rupture surface width was extended down-dip, and the slip within a layer extending from the surface to about 28 km depth was recovered. However, the uniform slip model calculated the depth of the Gerede earthquake rupture surface to be ~16 km. Both the studies using the recent GPS measurements and seismological data also reveal the thickness of the seismogenic layer to be ~16 km. The average crustal thickness is 31 ± 2 km in the study area. Therefore we suggest that the slip confined to the layer at depths between ~16 km and ~28 km may indicate postseismic afterslip and that asthenospheric relaxation continued for some time after the February 1, 1944 Gerede earthquake.

We have obtained here geologic and geodetic peak offsets of 7.16 m and 7.41 m, which are larger than previously reported values. The concentration of large offsets indicates that the likely epicentre location for the February 1, 1944 Gerede earthquake is just to the east of Gerede. We also calculated a geodetic recurrence interval of 232 ± 25 yr which agrees with the geologic recurrence interval of 266 ± 35 yr for large earthquakes to be sourced from the Gerede fault zone.

Table 5. The February 1, 1944 Gerede earthquake seismological and rupture surface parameters. M_s and M_w in brackets are computed from M_o using formulas $M_s = (2/3)(\log_{10}(M_o) - 16.14)$ (Ekström & Dziewonski 1988) and $M_w = (2/3)\log_{10}(M_o/1.e7) - 6$ (WGCEP, 1995) where M_o is in dyne.cm. M_o in brackets is computed from given either M_s or M_w. Latitude and longitude are epicentre coordinates. [a]– Computed using distributed slip model with width of 32 km.

References	Data Type	Latitude (°)	Longitude (°)	Strike (°)	Length (km)	Width (km)	Dip (°)	Average Strike Slip(m)	Average Dip Slip(m)	Maximum Strike Slip(m)	M_s	M_w	M_o (10^{20}Nm)
Ketin (1948); Ergin *et al.* (1967); Ketin (1969)	Geologic Isoseismal	40.8	32.2	75	180	–	–	–	1	3.5	7.4	(7.49)	(1.74)
Ambraseys & Zatopek (1969); Ambraseys (1970)	Geologic	41	33	75	190	–	–	–	–	3.5	7.6	(7.69)	(3.47)
Dewey (1976)	Seismic	41.1	33.22	–	–	–	–	–	–	–	7.3	(7.39)	(1.23)
Bonilla *et al.* (1984); Lienkaemper (1984)	Seismic Geologic	–	–	–	177	–	–	–	–	–	7.52	(7.55)	(2.63)
Jackson & McKenzie (1988)	Seismic	41.1	33.2	75	–	21.6	90	–	–	–	7.4	(7.56-7.76)	2.16-4.31
Wells & Coppersmith (1994)	Seismic Geologic	–	–	–	180	20	–	–	–	3.6	7.5	7.59	2.7
Wells & Coppersmith (1994)	Empirical Regression	–	–	–	191	21.04	–	4.2	–	8.25	(7.62)	7.71	(3.67)
Ambraseys & Jackson (1998)	Geologic	40.9	32.6	75	160	–	–	–	1	3.7	7.3	(7.39)	(1.23)
Kondo *et al.* (2005)	Geologic	–	–	–	180	–	–	3.4	–	6.3	–	–	–
This paper	Geologic	–	–	75	195	–	–	4.37	–	7.16	–	–	–
This paper Uniform Slip	Geodetic	40.81	32.23	76	191	16	85	4.4 ± 0.11	1.02 ± 0.17	7.41[a]	(7.65)	7.74	4.02

Acknowledgments

This research was partly supported by General Command of Mapping (GCM), Turkey, TÜBİTAK-INTAG 910 and TÜBİTAK-YDABAG 102Y053 grants. We thank Coşkun Demir and Mehmet Açikgöz of GCM for carrying out adjustment of triangulation network and processing GPS data. The English of the final text is edited by John A. Winchester.

References

Aktuğ, B., Ayhan, M.E. & Demİr, C. 2004. *Processing GPS Campaigns from 1992 to 2004 and Velocity Field of Turkey*. General Command of Mapping (GCM), Report no. **UZYTEK.-05-2004** [in Turkish].

Ambraseys, N.N. 1970. Some characteristic features of the Anatolian Fault Zone. *Tectonophysics* **9**, 143–165.

Ambraseys, N.N. 1988. Engineering seismology. *Journal of Earthquake Engineering and Structural Dynamics* **17**, 1–106.

Ambraseys, N.N. & Jackson, J.A. 1998. Faulting associated with historical and recent earthquakes in the Eastern Mediterranean region. *Geophysical Journal International* **133**, 390–406.

Ambraseys, N.N. & Zatopek, A. 1969. The Mudurnu Valley, West Anatolia, Turkey, earthquake of 22 July 1967. *Bulletin of Seismological Society of America* **59**, 521–589.

Arnadottir, T. & Segall, P. 1994. The 1989 Loma Prieta earthquake imaged from inversion of geodetic data. *Journal of Geophysical Research* **99** (B11), 21835–21855.

Aslan, E., Tezucan, L. & Bath, M. 1975. *An Earthquake Catalogue for Turkey for the Interval 1913–1970*. Kandilli Observatory Seismological Institute, Report no. **7–75**.

Ayhan, M.E., Demİr, C., Lenk, O., Kiliçoğlu, A., Altiner, Y., Barka, A., Ergİntav, S. & Özener, H. 2002. Interseismic strain accumulation in the Marmara Sea Region. *Bulletin of Seismological Society of America* **92**, 216–229.

Aytun, A. 1980. Creep measurements in the İsmetpaşa region of the North Anatolian Fault Zone. *In*: Işikara, A.M. & Vogel, A. (eds), *Multidisciplinary Approach to Earthquake Prediction.* Proceedings of the International Symposium on Earthquake Prediction in the North Anatolian Fault Zone. held in İstanbul, March 31–April 5 1980, 279–292.

Bandel, K. 1981. New stratigraphic and structural evidence for lateral dislocation in the Jordan rift connected with description of the Jurassic rock column in Jordan. *Neues Jahrbuch für Geologie und Palaontologie, Abhandlungen* **161**, 271–308.

Barka, A.A. 1996. Slip distribution along the North Anatolian Fault associated with large earthquakes of the period 1939 to 1967. *Bulletin of Seismological Society of America* **86**, 1238–1254.

Bonilla, M.G., Mark, R.K. & Lienkaemper, J.J. 1984. *Statistical Relations Among Earthquake Magnitude, Surface Rupture Length, and Surface Fault Displacement.* USGS, Open-File Report **84–256**, 33.

Bonilla, M.G. 1988. Minimum earthquake magnitude associated with coseismic surface faulting. *Bulletin of the Association of Engineering Geology* **XXV**, 17–29.

Bozkurt, E. 2001. Neotectonics of Turkey–a synthesis. *Geodinamica Acta* **14**, 3–30.

Çakir, Z., Akoğlu, A.M., Belabbes, S., Ergİntav, S. & Meghraoui, M. 2005. Creeping along the İsmetpaşa section of the North Anatolian Fault (Western Turkey): rate and extent from InSAR. *Earth and Planetary Science Letters* **238**, 225–234.

Demİrtaş, R. 2000. *Neotectonics and Paleoseismicity of the Section Between Abant and Gerede of the North Anatolian Fault Zone*. PhD Thesis, Ankara University, Ankara [in Turkish with English abstract, unpublished].

Dewey, J.F. 1976. Seismisity of Northern Anatolia. *Bulletin of Seismological Society of America* **66**, 843–868.

Dong, D., Herring, T.A. & King, R.W. 1998. Estimating regional deformation from a combination of space and terrestrial geodetic data. *Journal of Geodesy* **72**, 200–214.

Drews, A.R. & Snay, R.A., 1989. DYNAP: A software for estimating crustal deformation from geodetic data. *Tectonophysics* **162**, 331–343.

Du, Y., Aydin, A. & Segall, P. 1992. Comparison of various inversion techniques as applied to the determination of a geophysical deformation model for the 1983 Borah Peak earthquake. *Bulletin of Seismological Society of America* **82**, 1840–1866.

Du, Y., Segall, P. & Gao, H. 1997. Quasi-static dislocations in the three dimensional inhomogeneous media. *Geophysical Research Letters* **24**, 2347–2350.

Ekström, G. & Dziewonski, A.M. 1988. Evidence of bias in estimations of earthquake size. *Nature* **332**, 319–323.

Ergİn, K., Güçlü, U. & Uz, Z. 1967. *Earthquakes Catalogue within Turkey and Its Surrounding (BS 11 – 1964)*. Technical University of İstanbul, Mining Faculty, Geophysics Institute, no. **24** [in Turkish].

Feigl, K.L. & Thatcher, W. 2006. Geodetic observations of post-seismic transients in the context of the earthquake deformation cycle. *Geoscience* **338**, 1012–1028.

Freund, R., Garfunkel, Z., Zak, I., Goldberg, M., Weissbrod, T. & Derİn, B. 1970. The shear along the Dead Sea rift. *Philosophical Transactions of the Royal Society of London* **267**, 107–130.

Gençoğlu, S., İnan, E. & Güler, H. 1990. *Earthquake Hazard of Turkey*. Publication of the Chamber of Geophysical Engineers of Turkey, Ankara [in Turkish].

Harris, R.A. & Segall, P. 1987. Detection of a locked zone at depth on the Parkfield, California, segment of the San Andreas Fault. *Journal of Geophysical Research* **92** (B8), 7945–7962.

Hearn, E.H., Hager, B.H. & Reilinger, R.E. 2002. Viscoelastic deformation from North Anatolian Fault Zone earthquakes and the eastern Mediterranean GPS velocity field. *Geophysical Research Letters* **29**, doi: 10.1029/2002GL014889.

Hearn, E.H. & Burgmann, R. 2005. The effects of elastic layering on inversions of GPS data for coseismic slip and resulting stress changes: strike slip earthquakes. *Bulletin of Seismological Society of America* **95**, 1637–1653.

Hreinsdottir, S., Freymuller, J., Fletcher, H.J., Larsen, C.F. & Burgmann, R. 2003. Coseismic slip distribution of the 2002 Mw7.9 Denali fault earthquake, Alaska, determined from GPS measurements. *Geophysical Research Letters* **30**, doi: doi:10.1029/2003GL017447.

Hempton, M.R. 1987. Constraints on Arabian plate motion and extensional history of the Red Sea. *Tectonics* **6**, 687–705.

Herece, E. 2005. *Neotectonics of the Western Section of the North Anatolian Fault Zone*. PhD Thesis, Ankara University, Ankara [in Turkish with English abstract, unpublished]

Herring, T.A. 1998. *GAMIT/GLOBK Kalman Filter VLBI and GPS Analysis Program: V 4.1*. Massachusetts Institute of Technology.

Jackson, J. & Mckenzie, D.P. 1988. The relationship between plate motions and seismic moment tensors, and the rates of active deformation in the Mediterranean and Middle East. *Geophysical Journal of Royal Astronomical Society* **93**, 45–73.

Johnson, K.M., Hsu, Y.-J., Segall, P. & Yu, S.-B. 2001. Fault geometry and slip distribution of the 1999 Chi-Chi, Taiwan earthquake imaged from inversion of GPS data. *Geophysical Research Letters* **28**, 2285–2288.

Kalafat, D. 1998. Investigation of tectonic structures in Anatolia using earthquake mechanism. *Earthquake Research. Bulletin* **77**, 1–217 [in Turkish].

Keller, E.A & Pinter, N. 1996. *Active Tectonics: Earthquakes, Uplift and Landforms*. Prentice Hall.

Kenner, S.J. & Segall, P. 2000. Postseismic deformation following the 1906 San Francisco earthquake. *Journal of Geophysical Research* **105** (B6), 13195–13209.

Ketin, İ. 1948. On large earthquakes occurred in Turkey in last decade: tectonic and mechanic implications. *Bulletin of Turkish Geology Society* **II**, 1–13 [in Turkish with English abstract].

Ketin, İ. 1969. On the North Anatolian Fault. *Bulletin of Mineral Research Institute* **72**, 1–26 [in Turkish with English abstract].

Kiratzi, A.A. 1993. A study of active crustal deformation of the North and East Anatolian Fault zones. *Tectonophysics* **225**, 191–203.

Koçyiğit, A. 1987. Stratigraphy and nature of the northern margin of the Karabük-Safranbolu Tertiary basin. *Bulletin of Turkish Geology Society* **30**, 61–69 [in Turkish with English abstract].

Koçyiğit, A. 2005. The Denizli graben-horst system and the eastern limit of western Anatolian continental extension: basin fill, structure, deformational mode, throw amount and episodic evolutionary history, SW Turkey. *Geodinamica Acta* **18**, 167–208.

Koçyiğit, A. & Beyhan, A. 1998. A new intracontinental transcurrent structure: the Central Anatolian Fault Zone, Turkey. *Tectonophysics* **284**, 317–336.

Koçyiğit, A., Yusufoğlu, H. & Bozkurt, E. 1999. Evidence from the Gediz Graben for episodic two-stage extension in western Turkey. *Journal of the Geological Society*, *London* **156**, 605–616.

Koçyiğit, A., Yilmaz, A., Adamia, S. & Kuloshvili, S. 2001. Neotectonics of East Anatolian Plateau (Turkey) and Lesser Caucasus: implication for transition from thrusting to strike-slip faulting. *Geodinamica Acta* **14**, 177–195.

Koçyiğit, A., Ayhan, M.E., Çetin, H., Aktuğ, B., Aytun, A., Demir, C., Lenk, O., Kiliçoğlu, A., Açikgöz, M., Deveci, S., Biryol, B., Arca, S., Akturk, O. & Günaydin, O. 2006. *Earthquake Hazards of the Section Between İsmetpaşa-Gerede and Mengen of the North Anatolian Fault System (NAFS)*. TÜBİTAK-YDABAG-102Y053 project report [in Turkish with English abstract, unpublished].

Kondo, H., Awata, Y., Emre, O., Doğan, A., Özalp, S., Tokay, F., Yildirim, C., Yoshioka, T. & Okumura, K. 2005. Slip distribution, fault geometry and fault segmentation of the 1944 Bolu-Gerede earthquake rupture, North Anatolian Fault, Turkey. *Bulletin of Seismological Society of America* **95**, 1234–1249.

Lawson, C.L. & Hanson, R.J. 1974. *Solving Least Squares Problems.* Prentice-Hall, Englewood Cliffs, New Jersey.

Lienkaemper, J.J. 1984. Comparison of two surface-wave magnitude scales: M of Gutenberg and Richter (1954) and M_s of 'Preliminary determination of epicenter'. *Bulletin of Seismological Society of America* **74**, 2357–2378.

Mart, Y. 1991. The Dead Sea rift: from continental rift to incipient ocean. *Tectonophysics* **197**, 155–179.

McCarthy, D.D. & Petit, G. 2004. *IERS Conventions (2003)*. IERS Technical Note 32, Verlag des Bundesamts für Kartogrf. und Geod., Frankfurt.

Mcclusky, S., Balassanian, S., Barka, A., Demir, C., Ergintav, S., Georgiev, I., Gurkan, O., Hamburger, M., Hurst, K., Kahle, G.H., Kastens, K., Kekelidze, G., King, R., Kotzev, V., Lenk, O., Mahmoud, S., Mishin, A., Nadariya, M., Ouzounis, A., Paradissis, D., Peter, Y., Prilepin, M., Reilinger, R., Sanli, I., Seeger, H., Tealeb, A., Toksoz, M.N. & Veis, G. 2000. Global Positioning System constrains on plate kinematics and dynamics in the eastern Mediterranean and Caucasus. *Journal of Geophysical Research* **105** (B3), 5695–5719.

McKenzie, D.P. 1972. Active tectonics of the Mediterranean region. *Geophysical Journal of Royal Astronomical Society* **55**, 217–254.

Meade, B.J., Hager, B.H., Mcclusky, S.C., Reilinger, R.E., Ergintav, S., Lenk, O., Barka, A.A. & Özener, H. 2002. Estimates of seismic potential in the Marmara Sea Region from block models of secular deformation constrained by Global Positioning System measurements. *Bulletin of Seismological Society of America* **92**, 208–215.

Nakiboğlu, S.M., Ayhan, M.E., Demir, C., Kiliçoğlu, A. & Şanli, I. 1998. *Crustal Motion Within the Western Section of the North Anatolian Fault: Geodetic Observations and Geophysical Interpretations*. TUBİTAK-Intag 910 [in Turkish with English Abstract, unpublished].

Okada, Y. 1985. Surface deformation due to shear and tensile faults in a half space. *Bulletin of Seismological Society of America* **7**, 1135–1154.

Örgülü, G. & Aktar, M. 2001. Regional moment tensor inversion for strong aftershocks of the August 17, 1999 İzmit earthquake (Mw= 7.4). *Geophysical Research Letters* **28**, 371–374.

Özalaybey, S., Ergin, M., Aktar, M., Tapirdamaz, C., Biçmen, F. & Yörük, A. 2002. The 1999 İzmit earthquake sequence in Turkey: seismological and tectonic aspects. *Bulletin of Seismological Society of America* **92**, 376–386.

Öztürk, A., İnan, S. & Tutkun, Z. 1984. North Anatolian Fault Zone between Abant and Yeniçağa. *Cumhuriyet University, Faculty of Engineering, Journal of Earth Sciences* **1**, 1–18 [in Turkish with English Abstract].

Pinar, N. & Lahn, E. 1952. *Catalogue of Earthquakes in Turkey*. Ministry of Public and Housing Works, Ankara, **6**, 1–36 [in Turkish].

Pinar, A., Honkura, Y. & Kikuchi, M. 1996. A rupture model for the 1967 Mudurnu Valley, Turkey earthquake and its implication for seismotectonics in the western part of the North Anatolian Fault Zone. *Geophysical Research Letters* **23**, 29–32.

Quennell, A.M. 1958. The structural and geomorphic evolution of the Dead Sea rift. *Quarterly Journal of the Geological Society, London* **114**, 1–24.

Reilinger, R.E., Ergintav, S., Bürgmann, R., Mcclusky, S., Lenk, O., Barka, A., Gürkan, O., Hearn, L., Feigl, K.L., Çakmak, R., Aktuğ, B., Özener, H. & Toksöz, M.N. 2000. Coseismic and post processing fault slip for the 17 August 1999, M= 7.5.,İzmit, Turkey. *Science* **289**, 1519–1524.

Reilinger, R.E., Mcclusky, S., Vernant, P., Lawrance, S., Ergintav, S., Çakmak, R., Özener, H., Kadirov, F., Guliev, I., Stepanyan, R., Nadariya, M., Habubia, G., Mahmoud, S., Sakr, K., Arrajehi, A., Paradiskis, D., Al-Aydrus, A., Prilepin, M., Guseva, T., Evren, E., Dmitrotsa, A., Filikov, S.V., Gomez, F., Al-Ghazzi, R. & Karam, G. 2006. GPS constraints on continental deformation in Africa-Arabia-Eurasia continental collision zone and implications for the dynamics of plate interactions. *Journal of Geophysical Res*earch **111**, B05411.

Rothacher, M. & Mervart, L. 1996. *Bernesse GPS software: Version 4.0*. Astron. Ins., University of Bern.

Şengör, A.M.C., Görür, N. & Şaroğlu, F. 1985. Strike-slip faulting and related basin formation in zones of tectonic escape: Turkey as a case study. *In*: Biddle, K.T. & Christie-Blick, N. (eds), *Strike-Slip Deformation, Basin Formation and Sedimentation*. Society of Economic Paleontologists and Mineralogists, Tulsa, Special Publications **37**, 227–264.

Şengör, A.M.C., Tüysüz, O., İmren, C., Sakinç, M., Eyidoğan, H., Görür, N., Le Pichon, X. & Rangin, C. 2004. The North Anatolian Fault: a new look. *Annual Review of Earth and Planetary Sciences* **33**, 1–75.

Taşman, C.E. 1944. The Gerede-Bolu earthquake. *Bulletin of Mineral Research Institute***1**, 134–139 [in Turkish].

Ten Veen, J.H. 2004. Extension of Hellenic forearc shear zones in SW Turkey: The Pliocene–Quaternary deformation of the Eşençay Basin. *Journal of Geodynamics* **37**, 181–204.

Ten Veen, J.H. & Kleinspehn, K. 2002. Geodynamics along an increasingly curved convergent plate margin: Late Miocene–Pleistocene Rhodes, Greece. *Tectonics* **21**, doi: 10.1029/2001TC001287.

Ten Veen, J.H. & Kleinspehn, K. 2003. Incipient continental collision and plate boundary curvature: Late Pliocene–Holocene transtensional Hellenic forearc, Crete, Greece. *Journal of the Geological Society, London* **160**, 161–181.

Ten Veen, J.H., Woodside, J.M., Zitter, T.A.C., Dumont, J.F., Mascle, J. & Volkonskaia, A. 2004. Neotectonic evolution of the Anaximander Mountains at the Junction of the Hellenic and Cyprus arcs. *Tectonophysics* **391**, 35–65.

Thatcher, W. 1975. Strain accumulation and release mechanics of the 1906 San Francisco earthquakes. *Journal of Geophysical Research* **80**, 4862–4872.

Thatcher, W. & Lisowski, M. 1987. Long-term seismic potential of the San Andreas Fault southeast of San Francisco, California. *Journal of Geophysical Research* **92** (B6), 4771–4784.

Thatcher, W., Marshall, G. & Lisowski, M. 1997. Resolution of fault slip along the 470 km long rupture of the great 1906 San Francisco earthquake and its implications. *Journal of Geophysical Research* **102** (B3), 5353–5367.

Tibi, R., Bock, G., Xia, Y., Baumbach, M., Grosser, H., Milkereit, C., Karakisa, S., Zunbul, S., Kind, P. & Zschau, J. 2001. Rupture processes of the 1999 August 17 İzmit and November 12 Düzce (Turkey) earthquakes. *Geophysical Journal International* **144**, F1–F7.

Tokay, M. 1973. Geologic observations along the North Anatolian Fault Zone from Gerede to Ilgaz. *In: Proceedings of the Symposium on North Anatolian Fault Zone and Earthquake Belt*. Mineral Research Institute Publication, Ankara, 12–29 [in Turkish].

Walley, C.D. 1988. A new class of faults and their bearing on continental drift. *Nature* **207**, 343–347.

Wang, R., Martin, F.L. & Roth, F. 2003. Computation of deformation induced by earthquakes in a multi-layer elastic crus-FORTRAN programs EDGRN/EDCMP. *Computer & Geosciences* **29**, 195–207.

Wells, D.L. & Coppersmith, K.J. 1994. New empirical relationships among magnitude, rupture length, rupture width, rupture area, and surface displacement. *Bulletin of Seismological Society of America* **84**, 974–1002.

Wgcep 1995. Seismic hazards in Southern California: probable earthquakes, 1994 to 2024. *Bulletin of Seismological Society of America* **85**, 379–439.

Zor, E., Özalaybey, S. & Gürbüz, C. 2006. The crustal structure of the eastern Marmara region, Turkey by teleseismic receiver functions. *Geophysical Journal International* **167**, 213–222.